J Biol Inorg Chem (2014) 19:297–318
DOI 10.1007/s00775-013-1084-3

MINIREVIEW

High-frequency and high-field electron paramagnetic resonance (HFEPR): a new spectroscopic tool for bioinorganic chemistry

Joshua Telser · J. Krzystek · Andrew Ozarowski

Received: 10 September 2013 / Accepted: 27 December 2013 / Published online: 30 January 2014

Abstract This minireview describes high-frequency and high-field electron paramagnetic resonance (HFEPR) spectroscopy in the context of its application to bioinorganic chemistry, specifically to metalloproteins and model compounds. HFEPR is defined as frequencies above ~100 GHz (i.e., above W-band) and a resonant field reaching 25 T and above. The ability of HFEPR to provide high-resolution determination of g values of $S = 1/2$ is shown; however, the main aim of the minireview is to demonstrate how HFEPR can extract spin Hamiltonian parameters [zero-field splitting (zfs) and g values] for species with $S > 1/2$ with an accuracy and precision unrivalled by other physical methods. Background theory on the nature of zfs in $S = 1$, 3/2, 2, and 5/2 systems is presented, along with selected examples of HFEPR spectroscopy of each that are relevant to bioinorganic chemistry. The minireview also provides some suggestions of specific systems in bioinorganic chemistry where HFEPR could be rewardingly applied, in the hope of inspiring workers in this area.

Keywords Electron paramagnetic resonance · EPR · HFEPR · Metalloproteins · Bioinorganic model compounds · ENDOR · Mössbauer spectroscopy

Electronic supplementary material The online version of this article (doi:10.1007/s00775-013-1084-3) contains supplementary material, which is available to authorized users.

J. Telser (✉)
Department of Biological, Chemical and Physical Sciences, Roosevelt University, Chicago, IL 60605, USA
e-mail: jtelser@roosevelt.edu

J. Krzystek · A. Ozarowski
National High Magnetic Field Laboratory (NHMFL), Florida State University, Tallahassee, FL 32310, USA

Introduction

General overview

Electron paramagnetic resonance (EPR) spectroscopy, also known as electron spin resonance (ESR) or simply electron magnetic resonance (EMR), is an extremely powerful physical method employed in bioinorganic chemistry [1], among many other chemically and biologically related areas [2]. Chemistry is about electrons, and EPR directly provides information on electrons, albeit only when they are unpaired. From a bioinorganic point of view, this information is related to the identity, coordination geometry, spin state, metal oxidation state, bonding covalency, and other electronic aspects of a metal cofactor or biologically relevant metal complex.

The EPR technique has been described in detail in many texts, both general [1, 3] and specialized [4–7]. We should also point out two recent volumes in the series *Biological Magnetic Resonance* that focus on the applications of all forms of EPR [i.e., including electron nuclear double resonance (ENDOR) and electron spin echo envelope modulation (ESEEM)] to the full range of bioinorganic systems [8, 9]. In this minireview, we will assume a knowledge of the basics of EPR as it is commonly performed, and focus on the extension of this technique to high resonant energies (frequencies) and magnetic fields, along with applications to systems with $S > 1/2$. We refer to this variant of EPR as high-frequency and high-field EPR (HFEPR). Ten years ago, a *JBIC* minireview on this topic was published [10], and a volume of *Biological Magnetic Resonance* focused on it [11], but subsequent technological developments in the field and in the breadth of systems to which it has been applied warrant a more up-to-date review of this topic. We also believe that it would be useful to summarize briefly the salient characteristics of the various systems with $1 \leq S \leq 5/2$.

One might naively assume that merely extending the resonant frequency and associated external magnetic field strength would not be "game changing." This is not the case. Although the basics of EPR are the same regardless of frequency/field, HFEPR requires significant changes not only in instrumentation, but also in interpretation and in the selection of systems that are most appropriate for study. We can begin by considering the better known technique of nuclear magnetic resonance (NMR). Over the years, the resonant frequency for NMR has shifted from 60 MHz to 90–100 MHz to 300–400 MHz and, most recently, to 600–1000 MHz. However, these all lie within the radio-frequency regime, so no major changes in technology have been required even though the magnets have changed from resistive (electro)magnets to superconducting magnets, with very high fields now employed (23.5 T for ^{1}H NMR at 1 GHz). The other change in NMR has been that from continuous wave (CW) operation exclusively to pulsed (time domain with Fourier transform) operation. The advantages of these developments are many, and their enumeration is far beyond the scope of this minireview. There is however, one relevant aspect of the upwards march of NMR frequencies: the much greater dispersion of NMR signals, which allows resolution among species with similar chemical shifts, whatever the dimensional technique used.

The situation is somewhat different in EPR. While the quest for ever higher combinations of frequency and field has resulted in similar changes in magnet technology to those seen in NMR, with the use of superconducting and occasionally resistive Bitter-type solenoid magnets, the frequencies applied exceed what is commonly termed the microwave range and venture into the sub-THz region, reaching values close to 1 THz. This requires a fundamental change in the methods of generating, propagating, and detecting the electromagnetic radiation, since conventional technology such as that used in X- or Q-band EPR is no longer applicable. This has far-reaching consequences for the practical use of HFEPR in bioinorganic chemistry, which will be covered in the section "Practical aspects of HFEPR spectroscopy" later on. Also, unlike in NMR, a vast majority of HFEPR experiments are still performed in the CW mode (again because of technological reasons), although pulsed methods are being introduced [12, 13].

High-resolution HFEPR

In EPR, a similar situation to that observed for NMR occurs with an increase in field and frequency, namely an improvement in spectral resolution. This allows systems of interest, such as organic radicals, to have their g values determined with high accuracy, permitting similar species to be distinguished from each other and providing data for detailed calculations of electronic structure. This topic has been recently reviewed by Stoll [14] and will not be discussed further in this minireview, except to point out that organic radicals occur in many systems of bioinorganic interest, such as radical *S*-adenosylmethionine (SAM) enzymes [15–17], photosynthesis [18], and other systems [14]. The effects of an increase in resonant frequency/field on a given $S = 1/2$ EPR signal are described in detail by Stoll [14], but it is useful to illustrate them here for two important cases of amino-acid based radicals, tyrosine and tryptophan. For the tyrosyl radical, W-band is sufficient to resolve the **g** matrix, as shown in Fig. S1 of the Electronic Supplementary Material (ESM). However, for tryptophan radicals it is necessary to use much higher frequencies, reaching 400 GHz [19] or even 700 GHz [20], to achieve the desired resolution. This is demonstrated in Fig. 1, which uses the **g** matrix for a tryptophan radical in a tyrosine-depleted azurin mutant (AzC-W48), with $\mathbf{g} = [2.00361, 2.00270, 2.00215]$ [20]. Only at 700 GHz is the resolution sufficient to extract the g values fully. Such high frequencies are representative of those available at the National High Magnetic Field Laboratory (NHMFL) in Tallahassee, Florida and at the Grenoble High Field Laboratory, France, although similar equipment can increasingly be found elsewhere.

Broadband HFEPR

The primary application of HFEPR, however, has no direct analogy with NMR, and is closely related to the phenomenon known as zero-field splitting (zfs). The theoretical background of zfs will be presented in the next section. Zfs occurs only when $S > 1/2$, and results in the splitting of M_S levels (which would otherwise be degenerate) in zero magnetic field. Its presence leads to very strongly anisotropic EPR spectra: a zfs magnitude of 10 cm^{-1}, which is typical for transition metal complexes, causes a spread of resonances of over 40 T on the magnetic field scale for $S = 2$ when observed at 700 GHz. Moreover, many of those resonances cannot even be detected if the EPR frequency is much lower than that corresponding to the zfs, as will be shown below. The phenomenon of zfs therefore requires that (a) high frequencies are applied, in conjunction with high fields, and (b) multiple frequencies are used to dependably interpret the spectra, which are frequently very complicated. It should be mentioned at this point that HFEPR not only delivers the magnitude of zfs, but also—at low enough temperatures and high enough frequencies and fields—its sign, which is an important parameter related to the electronic structure of the given metal center. This will be discussed in more detail later.

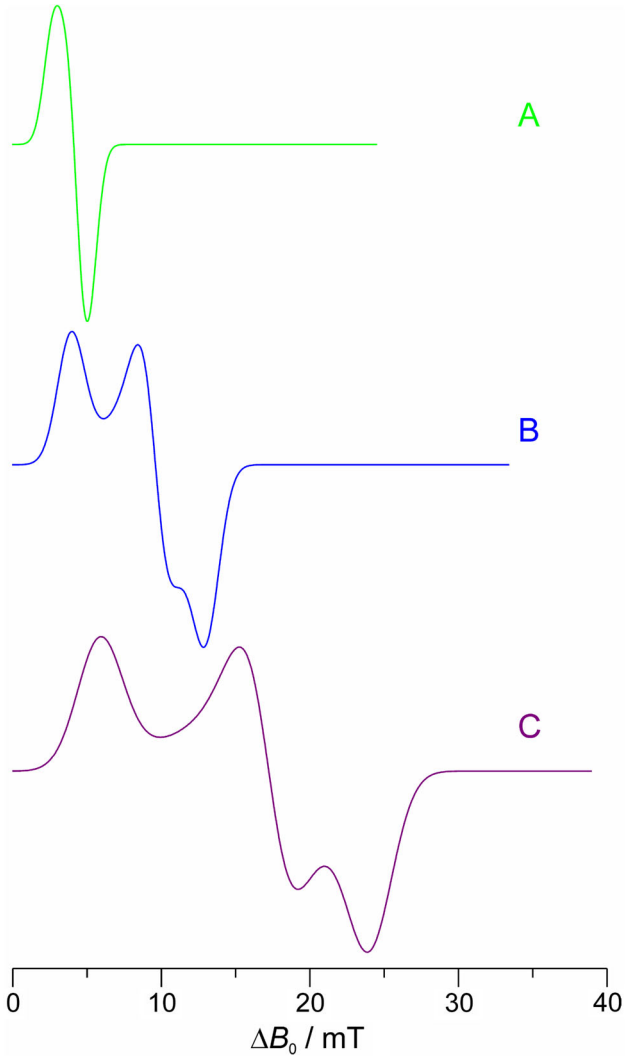

Fig. 1 Simulated powder pattern EPR spectra for a tryptophan radical in an azurin mutant ($\mathbf{g} = [2.00361, 2.00270, 2.00215]$) at various resonant frequencies: (*A*) W-band (95 GHz), (*B*) 350 GHz, and (*C*) 700 GHz. The spectra are offset ($\Delta B_0 = B_0 - B_{\text{offset}}$) such that the low-field edge of the $g_{\max}$ (2.00361) feature is set to zero field. The intensities are scaled to the same height for ease of comparison. The isotropic single-crystal EPR linewidths are increased with frequency, somewhat arbitrarily, to represent *g*-strain. The field offsets (in T) and linewidths (in MHz; Gaussian, hwhm) are: (*A*) 3.385, 20; (*B*) 12.477, 30; (*C*) 24.956, 50

Theoretical background: spin systems in zero field

The basics of zfs

In chemistry, one is concerned with nuclear spin angular momentum (quantum number, *I*), but not with any aspects of nuclear structure, which are in the realm of nuclear physics, aside from perhaps being reflected in the Larmor frequencies of the nuclei of NMR interest. In contrast, in EPR, one must consider not only the electronic spin angular momentum (quantum number *S*), but also the electronic orbital angular momentum (quantum number *L*). These two forms of angular momentum can interact via spin–orbit coupling (SOC), which leads to deviations of *g* values from that for a free electron ($g_e = 2.0023192$; see Eq. 1.11 in Anatole Abragam and Brebis Bleaney's classic text; hereafter referred to as "A^2B^2" [4]), as seen even for the tyrosyl radical mentioned above. For a *p*-block radical of that type, where all of the elements are light ($ns,p \leq 2$), these effects are small. When the radical is metal-centered ($ns,p \geq 3$), then these effects can be more pronounced due to the correlation of SOC with the number of electrons. For example, an organometallic Ge(I) ($[\text{Ar}]4s^2 3d^{10} 4p^1$, $S = 1/2$) species has $\mathbf{g} = [1.968, 1.997, 2.001]$ ($g_{\text{iso}} = 1.988$). The extreme cases are found in the *f*-block elements, where spin–orbit (Russell–Saunders, $J = |L - S|, \ldots$) coupling is the dominant factor and the *g* value depends on *L*, *S*, and *J* (see Eqs. 1.12, 1.13 in A^2B^2 [4] and 11–35 in Drago [3]).

Our concern in this minireview, however, is with *d*-block paramagnetic complexes, as these are of paramount interest in bioinorganic chemistry. In these cases, the *g* values for $S = 1/2$ systems can be highly variable, particularly for cases where there is a significant orbital contribution, such as for low-spin d^5 complexes [21, 22], as found in many Fe(III) porphyrins and heme enzymes [23]. HFEPR is of course not really needed in cases with such a wide dispersion of *g* values, although a high field is helpful for observing *g* values that are very low ($g < \sim 1$). HFEPR is, however, necessary when the spin–orbit interaction leads to significant zfs. A detailed description of this phenomenon is beyond the scope of this minireview, as it is described in many sources, both textbooks [3, 4, 6, 7] and review articles [24, 25]. The origin of zfs is in the mixing of excited electronic states with the ground state of the particular spin system via SOC, and also in the dipolar interactions between multiple electron spins in the given center (spin–spin coupling, SSC) [26].

Briefly, the interaction between spin and orbital angular momentum is given by the following Hamiltonian (see Eqs. 1.102, 103 in A^2B^2 [4]):

$$\mathcal{H} = \lambda(\hat{L} \cdot \hat{S}),$$

where λ is the multi-electron SOC constant, with $\lambda = \pm\left(\frac{\zeta}{2S}\right)$, and ζ is the single-electron SOC constant. The value of ζ is always positive; λ is positive for less than half-filled electron shells and negative for greater than half-filled shells. The optimal source for ζ values of *d*-block free ions is Bendix et al. [27]. SOC in, for example, a $3d^3$ free ion ($L = 3$, $S = 3/2$) gives a ${}^4F_{3/2}$ ($J = 3/2$) ground state with $J = 5/2$, $7/2$, and $9/2$ excited states at energies of, respectively, $(5/2)\lambda$, $(12/2)\lambda$, and $(21/2)\lambda$ above the ground

state, corresponding to hundreds of cm^{-1} (see Fig. 1.14 in A^2B^2 [4]). An example of how SOC leads to zfs will be given in the section "Relation between spin Hamiltonian parameters and bonding information."

In bioinorganic chemistry, however, we deal not with free ions but with complexes in which covalent bonding reduces the orbital contribution in general, and in which the symmetry is relatively low, so that this contribution is further reduced. As a result, a spin Hamiltonian can generally be used. The spin Hamiltonian, as its name implies, uses only the spin, S, while the orbital effects are incorporated into the g anisotropy and zfs parameters, as given in the following Hamiltonian (see Eq. 3.19 in A^2B^2 [4]):

$$\mathcal{H} = \beta_e(B \cdot g \cdot \hat{S}) + \sum_{k,q} B_k^q \hat{O}_k^q,$$

where the first term is the electronic Zeeman interaction, β_e is the Bohr magneton (9.2740×10^{-24} J/T), and the second term includes a variety of orders of zfs interactions (B_k^q is the energy parameter and $\hat{O}_k^q$ is the spin operator; see Tables 16 and 17 in A^2B^2 [4]), with higher-order terms possible for higher spins, $k = 0$ (i.e., no zfs) for $S = 1/2$; $k = 2$ for $S \geq 1$, $k = 4$ for $S \geq 2$, and $k = 6$ for $S \geq 3$. The values of q depend on the symmetry of the spin system. Papers by McGavin are recommended for extensive discussions of these effects [28, 29]. For bioinorganic systems, it is generally sufficient to consider only the second-order terms, so that this Hamiltonian can be rewritten in the more familiar form (see Eqs. 3.26 and 3.27 in A^2B^2 [4])

$$\mathcal{H} = \beta_e(B \cdot g \cdot \hat{S}) + D\left\{\hat{S}_z^2 - \frac{1}{3}S(S+1)\right\} + E(\hat{S}_x^2 - \hat{S}_y^2),$$

where D $(3B_2^0)$ is the (uni)axial zfs parameter and E (B_2^2) is the rhombic zfs parameter. The former is present when $z \neq x$, y; the latter is present when $z \neq x \neq y$. An equivalent form of this equation, which is often seen, is (see Eqs. 3.24 and 3.25 in A^2B^2 [4])

$$\mathcal{H} = \beta_e(B \cdot g \cdot \hat{S}) + \hat{S} \cdot \boldsymbol{D} \cdot \hat{S},$$

where the $\boldsymbol{D}$ tensor components (D_x, D_y, D_z) can be related to D and E as follows:

$$D = \frac{3}{2}D_z, \quad E = \frac{1}{2}(D_x - D_y).$$

This interaction leads to different energies, even in the absence of an external magnetic field, for different magnitudes of spin projection. These effects will be described for each of the following cases: $S = 1$, 3/2, 2, and 5/2, all of which are relevant to mononuclear metal centers and many di- and polynuclear centers in bioinorganic chemistry. Still higher spins are possible when there are magnetically interacting d-block ions, such as $S = 9/2$, observed for a 2Fe ferredoxin [30] and in a model compound [31], but these situations are rare enough to be ignored here.

The zero-field energy levels for $S = 1$, 3/2, 2, and 5/2 in the presence of zfs are shown together in Fig. 2 and will be discussed in ascending order in the following sections. Note that two of these are non-Kramers (integer spin) systems and two are Kramers (half-integer spin) systems. These two types of spin systems have different qualitative characteristics, as will be discussed below. Note that, by convention, the situation where the $\langle S, M_S|\langle S, \pm S|$ Kramers or non-Kramers doublet is the highest on the energy scale corresponds to a positive D, while the reverse is true for negative D.

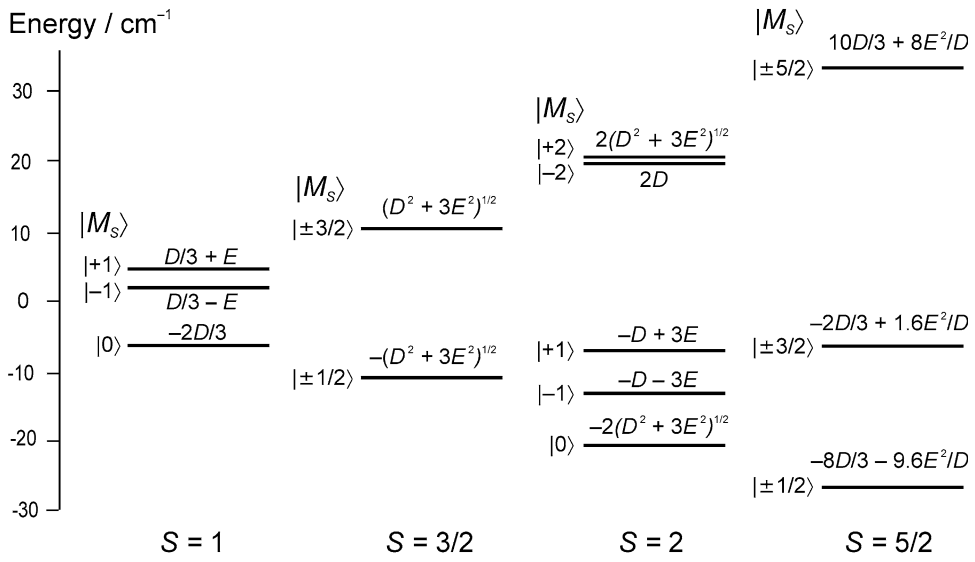

Fig. 2 Zero-field energy levels for the four most frequently encountered spin states in high-spin transition metal complexes. In each case, the same positive values of zfs parameters were used: $D = +10$ cm^{-1}, $E = +1$ cm^{-1} ($E/D = 0.1$). In the case of negative zfs, the level order is simply reversed. The energies for $S = 1$, 3/2, 2 are calculated using exact formulae; those for $S = 5/2$ are calculated through second-order perturbation theory

Spin triplets, $S = 1$

For $S = 1$ in cubic symmetry, the three spin levels $M_S = \pm 1$, 0 are degenerate in the absence of an external magnetic field, but with axial symmetry, the $M_S = \pm 1$ and 0 levels are split by D—the zfs. With rhombic symmetry, there is mixing between the $M_S = \pm 1$ states, which leads to the following energy levels given by W_{M_S} (see Eq. 3.28 in A^2B^2 [4]):

$$\langle S, M_S| = \langle 1, \pm 1| : W_{+1,-1} = +1/3\, D \pm E;$$
$$\langle S, M_S| = \langle 1, 0| : W_0 = -2/3\, D.$$

Thus, at zero field it is possible to measure both D and E directly.

Spin quartets, $S = 3/2$

For $S = 3/2$, $M_S = \pm 1/2$, $\pm 3/2$, and these four spin levels, in two Kramers doublets, are degenerate in the absence of zfs. However, with an axial zfs ($D > 0$), the energies of these levels are as follows:

$$\langle S, M_S| = \langle 3/2, \pm 3/2| : W_{3/2} = +D;$$
$$\langle S, M_S| = \langle 3/2, \pm 1/2| : W_{1/2} = -D.$$

With rhombic zfs, the energy separation at zero field, Δ, is

$$\Delta = 2\left\{D^2 + 3E^2\right\}^{1/2} = 2D\left\{1 + 3\left(\frac{E}{D}\right)^2\right\}^{1/2}.$$

The latter form is convenient if one specifically wants to define a rhombicity (E/D) term, which is often all that is directly extracted from other nonresonant physical methods, and has a maximum value of 1/3 in the standard formalism used here. Note that rhombic zfs mixes the $M_S = \pm 3/2$ and $\mp 1/2$ states equivalently, so that, in contrast to the case for $S = 1$, there is no ability at zero field to distinguish between axial and rhombic cases for $S = 3/2$; only a single value of Δ is observable.

Spin quintets, $S = 2$

For $S = 2$, the situation becomes more complicated as, in principle, one should now consider fourth-order zfs interactions: $\hat{O}_4^{0,2,3,4}$. These effects will be discussed later. With only axial second-order zfs, the zero-field energy levels for $S = 2$ are as follows:

$$\langle S, M_S| = \langle 2, \pm 2| : W_{\pm 2} = +2D;$$
$$\langle S, M_S| = \langle 2, \pm 1|, W_{\pm 1} = -D;$$
$$\langle S, M_S| = \langle 2, 0| : W_0 = -2D.$$

With a rhombic contribution, the situation is even more complicated (see Fig. 3.25 and Table 3.13 in A^2B^2 [4]), but there is still an exact solution:

$$\langle S, M_S| = \langle 2, \pm 2^s| : W_{\pm 2^s} = +2(D^2 + 3E^2)^{1/2}$$
$$= 2D\left\{1 + 3\left(\frac{E}{D}\right)^2\right\}^{1/2};$$
$$\langle S, M_S| = \langle 2, \pm 2^a| : W_{\pm 2^a} = +2D;$$
$$\langle S, M_S| = \langle 2, \pm 1^s| : W_{\pm 1^s} = -D + 3E;$$
$$\langle S, M_S| = \langle 2, \pm 1^a| : W_{\pm 1^a} = -D - 3E;$$
$$\langle S, M_S| = \langle 2, 0| : W_0 = -2(D^2 + 3E^2)^{1/2}$$
$$= -2D\left\{1 + 3\left(\frac{E}{D}\right)^2\right\}^{1/2}.$$

The splitting within the $M_S = \pm 1$ levels, if observable, allows E to be directly determined. There is also splitting within the $M_S = \pm 2$ levels (the zero-field designations 2^s and 2^a are more properly used), which will be discussed below.

Spin sextets, $S = 5/2$

For $S = 5/2$, the three Kramers doublets, $M_S = \pm 5/2$, $\pm 3/2$, $\pm 1/2$, give the following energies (relative energies in parentheses) with axial zfs:

$$\langle S, M_S| = \langle 5/2, \pm 5/2| : W_{\pm 5/2} = +\frac{10}{3}D\,(+6D);$$
$$\langle S, M_S| = \langle 5/2, \pm 3/2| : W_{\pm 3/2} = -\frac{2}{3}D\,(+2D);$$
$$\langle S, M_S| = \langle 5/2, \pm 1/2| : W_{\pm 1/2} = -\frac{8}{3}\,D(0).$$

As with $S = 2$, cubic zfs should be considered for $S = 5/2$, and is especially important in this case because high-spin d^5 is a spherically symmetric free ion ($L = 0$), so that zfs effects via SOC are usually small and arise from higher-order interactions [32]. This cubic zfs interaction is represented in various ways; one is to use the parameter a, which is defined as follows (see A^2B^2 Eq. 3.22 and Table 7.16 [4]):

$$a = 120B_4;$$
$$H_{\text{tetragonal}} = B_4\left\{\hat{O}_4^0 + 5\hat{O}_4^4\right\};$$
$$H_{\text{trigonal}} = -\frac{2}{3}B_4\left\{\hat{O}_4^0 + 20\sqrt{2}\hat{O}_4^3\right\}.$$

However, it is often more convenient to use the independent zfs parameters B_4^0 (this axial fourth-order zfs can also be defined as F, where $F = 180B_4^0$) and B_4^4 or B_4^3, the latter two for descriptions of the metal site using, respectively, tetragonal or trigonal symmetry models. When the symmetry is rhombic, the situation is too complex for an analytical solution (there are two cubic equations with roots that lack compact formulae), but second-order perturbation theory gives the following:

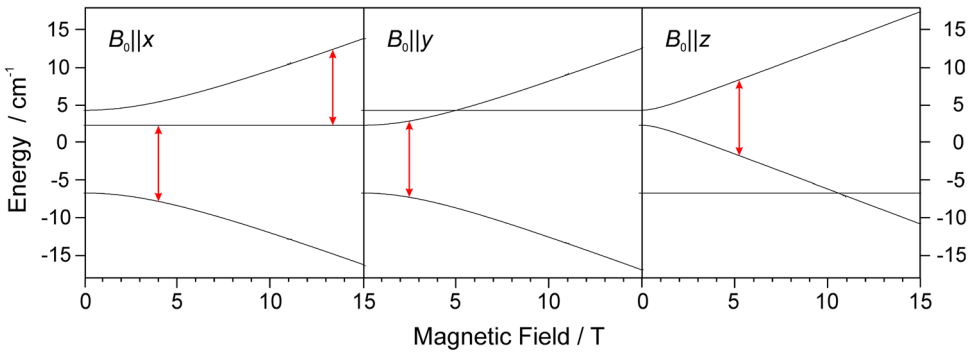

Fig. 3 Energy levels of a spin triplet ($S = 1$) as a function of the external applied magnetic field, with $D = +10$ cm^{-1}, $E = +1$ cm^{-1}, $g = 2.00$, for three canonical orientations of the zfs tensor relative to the magnetic field. Each *red arrow* indicates a microwave quantum of 300 GHz (10 cm^{-1}) and corresponds to a magnetic dipole allowed ($\Delta M_S = \pm 1$) transition. Note that an X-band microwave energy quantum (0.3 cm^{-1}) would excite transitions only in the regions where the spin sublevels cross over, i.e., at ca. 5 T for $B_0 \parallel y$ and 10.5 T for $B_0 \parallel z$; these fields are far too high for any standard X-band (or Q-band) spectrometer to reach

$$\langle S, M_S| = \langle 5/2, \pm 5/2| : W_{\pm 5/2} = +\frac{10}{3}D + 8.0\left(\frac{E^2}{D}\right);$$

$$\langle S, M_S| = \langle 5/2, \pm 3/2| : W_{\pm 3/2} = -\frac{2}{3}D + 1.6\left(\frac{E^2}{D}\right);$$

$$\langle S, M_S| = \langle 5/2, \pm 1/2| : W_{\pm 1/2} = -\frac{8}{3}D - 9.6\left(\frac{E^2}{D}\right).$$

The above equations, which to our knowledge have not appeared elsewhere, are accurate to within a few percent of an exact calculation (i.e., matrix diagonalization) for low rhombicity ($|E/D| \leq 0.1$).

Theoretical background: spin systems in an external magnetic field

All of the above discussion ignores the application of an external magnetic field, which is necessary for EPR to be observed. Thus, the electronic Zeeman effect makes for a situation that is best depicted graphically, as we will show for each of the above spin systems in turn.

$S = 1$ in a magnetic field

We present in Fig. 3 the energy levels as a function of the external magnetic field, B_0, for $S = 1$ with the field aligned along the molecular x, y, and z directions. The z direction is that of the axial zfs, defined by D; the "easy axis." The magnitude chosen, $|D| = 10$ cm^{-1}, is far larger than that seen for organic triplets [7], but is typical of transition metal complexes of the type we and others have investigated [33–35]. It can be easily seen that conventional microwave frequencies, even at W-band (95 GHz), are much too small to span the energy gap between the ground and excited spin levels. It is this phenomenon that has led to such systems being dubbed "EPR-silent." However, as can also be seen, if sufficient microwave energy is available in conjunction with resonant applied fields, then EPR spectra can be readily observed. Note that Fig. 3 presents the case for $D > 0$; $D < 0$ would invert the zero-field energies, but the results would be qualitatively the same.

In a randomly oriented (powder pattern) spin triplet, there can also be a resonant transition that is not aligned with the canonical directions shown in Fig. 3 and appears at a field below any of these. This feature is thus known as $B_{\min}$ (or $H_{\min}$ in older, non-SI literature), and is typically described as corresponding to a $\Delta M_S = 2$ transition.[1] It occurs at the following field (for an isotropic g, which is sufficient for most cases):

$$B_{\min} = \frac{1}{g\beta_e}\sqrt{\frac{1}{4}(h\nu)^2 - \frac{1}{3}D^2 - E^2}.$$

The signal intensity of $B_{\min}$ can sometimes be much larger than that of the $\Delta M_S = 1$ transition [7], as will be shown below.

$S = 3/2$ in a magnetic field

Figure 4 presents the corresponding situation for $S = 3/2$ with rhombic zfs. For $D > 0$, we have a system that is readily observable by conventional EPR, since the $\langle S, M_S| = \langle 3/2, \pm 1/2|$ Kramers doublet is the ground spin level, and the EPR transition within this doublet fulfills the $\Delta M_S = \pm 1$ condition and is therefore fully allowed. A famous example of such a situation is the resting state of nitrogenase iron-molybdenum cofactor (FeMoco), which has the following observed g matrix at X-band for the enzyme from *Azotobacter vinelandii* (*Av*): $\mathbf{g}' = [4.32,$

[1] A^2B^2 explains (p 155) [4] that this is more properly a $\Delta M_S = 0$ transition, as the $\langle S, M_S| = \langle 1, +1|$ and $\langle 1, -1|$ states are mixed, so that the transition is better described as $\langle 1, \pm 1| \leftrightarrow \langle 1, \pm 1|$, which is favored with $B_1 \parallel B_0$, than as $\langle 1, \pm 1| \leftrightarrow \langle 1, \mp 1|$.

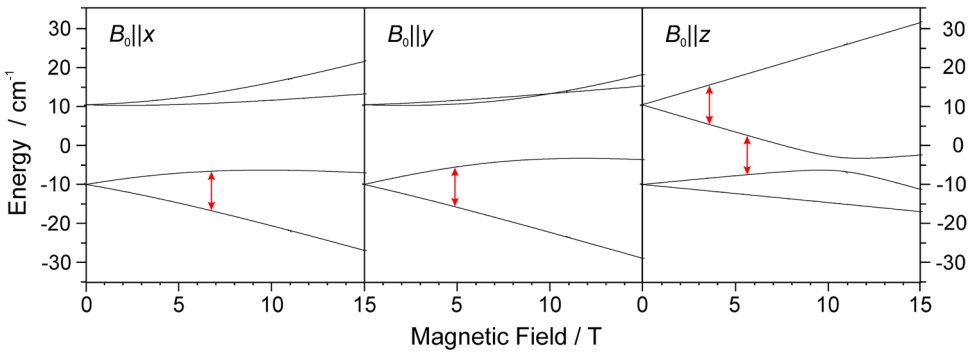

Fig. 4 Energy levels of a spin quartet ($S = 3/2$) as a function of the external applied magnetic field, with $D = +10$ cm^{-1}, $E = +1$ cm^{-1}, $g = 2.00$, for three canonical orientations of the zfs tensor relative to the magnetic field. Each *red arrow* indicates a microwave quantum of 300 GHz (10 cm^{-1}). Note that only intra-Kramers transitions are observed for $B_0 \parallel x$ and y, while a much more informative inter-Kramers resonance is also visible for $B_0 \parallel z$ at ca. 6 T, which in principle allows one to determine the zfs parameters of such a spin system

3.68, 2.01] [36, 37]. Such an EPR signal ($g'_\perp \approx 4$, $g'_\parallel \approx 2$) arises when $D > 0$ and $|D| \gg h\nu$, and the specific $g'_\perp$ values allow the determination of $|E/D|$. In this work by Hoffman and colleagues, it was possible to determine the complete $S = 3/2$ spin Hamiltonian parameters by combining the EPR data with ^{57}Fe ENDOR data to give $D = +6.07$ cm^{-1}, $|E| = 0.32$ cm^{-1}, $g_\perp = 2.005$, $g_\parallel = 2.01$ [36, 37]. How was this possible when $|D| \gg h\nu$, so that only transitions within the $M_S = \pm 1/2$ spin manifold can be observed? The accurate measurement of the Larmor splitting of the ^{57}Fe ENDOR signals allowed observation of the pseudonuclear Zeeman effect, wherein the Larmor (NMR) frequency of the ^{57}Fe ENDOR signals at $g'_\perp$ are shifted from that of an ordinary $S = 1/2$ case proportionally to $A_\perp/\Delta$, where A is the hyperfine coupling in the $S = 3/2$ representation (see also A^2B^2 Eqs. 1.100 and 4.54 [4]) [36, 37]. Thus, the full set of spin Hamiltonian parameters for a system where $|D| \gg h\nu$ was determined with only conventional fields/frequencies, but it was not achieved merely by EPR. The work required not only detailed ENDOR studies but isotopic enrichment in ^{57}Fe, and furthermore was successful because of the relatively large A values in this system; for small A (or large Δ), the shifts would be too small to be observed.

$S = 2$ in a magnetic field

We next come to $S = 2$ systems, which are of great importance in bioinorganic chemistry, as they include Fe(II) ($3d^6$, $S = 2$) present in many heme and non-heme Fe enzymes and in reduced di-iron oxo enzymes [38–40]. This is another instance where the system is often considered to be EPR-silent. This "silence" is strictly speaking the case only when $D \gg h\nu$, i.e., when the magnitude of D is large and positive, so that a situation similar to that shown in Fig. 3 occurs, albeit with another, higher energy, doublet ($M_S = \pm 2$). The effect of a magnetic field on $S = 2$ is shown in Fig. 5 for the case of a positive D.

As has been known for many years [41, 42], when the zfs is rhombic the $M_S = \pm 2$ states mix with the $M_S = 0$ state, and the former are split in zero field by a small amount (see A^2B^2 Eqs. 3.97–3.100 [4]). A partly allowed transition can occur within this doublet when in resonance with conventional EPR frequencies at very low applied fields (e.g., $B_0 \approx 10$ mT), and the signal is greatly enhanced when the oscillating magnetic field (i.e., B_1 from the microwave radiation) is parallel to B_0. The resonant energy ($h\nu$) required is (see A^2B^2 Eq. 3.100 [4])

$$h\nu = \left\{(\tilde{g}_\parallel \beta_e B \cos\theta)^2 + \Delta^2\right\}^{1/2}; \tilde{g}_\parallel = 4g_\parallel;$$

$$\Delta = \frac{12E^2}{(W_{\pm 2} - W_0)},$$

where θ is the angle between B_0 and the z axis ($g_\parallel$).

The parallel-mode detection technique at low frequencies has been very fruitfully applied to many bioinorganic $S = 2$ systems, chiefly those containing Fe(II) [43–45], but also Fe(IV) [46, 47] and Mn(III) [48] (both of which are $3d^4$, $S = 2$). These workers have shown that it is possible to extract the full set of spin Hamiltonian parameters from an analysis of this low field signal. However, we believe that caution is advisable when assuming that a unique set of parameters results from this single frequency (usually X-band; occasionally also with Q-band) measurement. Difficulties arise from the choice of $g_\parallel$, which may be problematic to determine independently from a range of $|E/D|$ values giving similar results, and from the omission of fourth-order terms, which mix the $M_S = \pm 2$ and ∓ 2 states directly (rather than via $M_S = 0$).

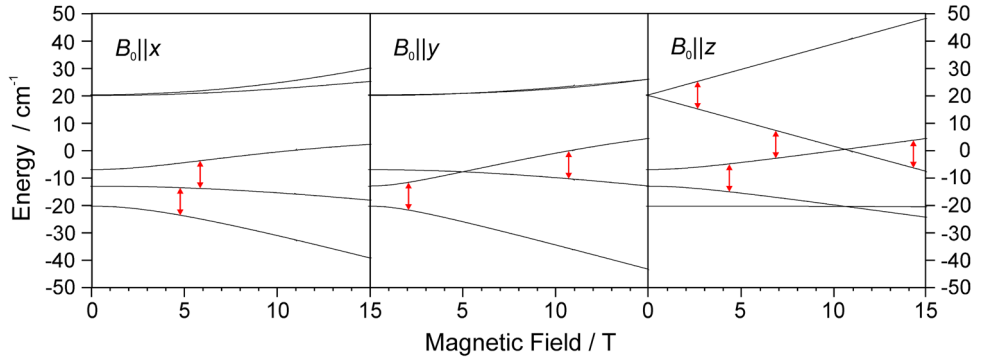

Fig. 5 Energy levels of a spin quintet ($S = 2$) as a function of the external applied magnetic field, with $D = +10$ cm^{-1}, $E = +1$ cm^{-1}, $g = 2.00$, for three canonical orientations of the zfs tensor relative to the magnetic field. Each *red arrow* indicates a microwave quantum of 300 GHz (10 cm^{-1}). The lowest field transition for $B_0 \parallel z$ is the only resonance observable at conventional frequencies (e.g., X-band) and is enhanced by using microwaves polarized so that $B_1 \parallel B_0$

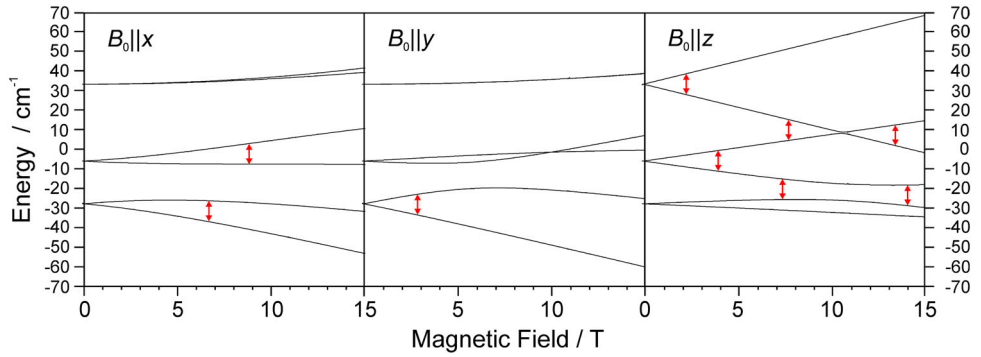

Fig. 6 Energy levels of a spin sextet ($S = 5/2$) as a function of the external applied magnetic field, with $D = +10$ cm^{-1}, $E = +1$ cm^{-1}, $g = 2.00$, for three canonical orientations of the zfs tensor relative to the magnetic field. Each *red arrow* indicates a microwave quantum of 300 GHz (10 cm^{-1}). Intra-Kramers transitions within the ground state doublet for each orientation would be observed at conventional frequencies

$S = 5/2$ in a magnetic field

For $S = 5/2$, a Kramers system, as with $S = 3/2$, we can easily observe EPR spectra using conventional fields, both when the zfs is small in magnitude—as is the case for Mn(II)—and when it is large, as long as $D > 0$ (that is, $\langle S, M_S| = \langle 5/2, \pm 1/2|$ Kramers doublet is the ground spin level, in which case $g'_{\perp} \approx 6$, $g'_{\parallel} \approx 2$). A classic example of the latter type is Fe(III) in hemes, such as in fluorometmyoglobin (met-Mb-F). In this complex, the pseudo-nuclear Zeeman effect, here seen in ^{19}F ENDOR signals, allowed the determination of D as $+6.1(1)$ cm^{-1} (this complex is essentially axial; this D value is for pH 6) [49]. The ability to perform high-resolution ENDOR spectroscopy, in combination with the large hyperfine coupling of ^{19}F, allowed this measurement of zfs, which is not generally applicable to $S = 5/2$ systems with large D values. The effect of the magnetic field on $S = 5/2$ is shown in Fig. 6.

For cubic zfs, there are analytical solutions for the energy levels when the magnetic field is along the three- or fourfold axis (see A^2B^2 Tables 3.1 and 3.2 [4]), but they will not be reproduced here. There are no useful analytical solutions for rhombic zfs with an applied field.

Lastly, a feature worth noting is the "junk iron" signal that appears at $g_{\text{eff}} \approx 4.3$ for systems with large $|E/D|$. This was fully explained many years ago by Aasa, who gave perturbation theory expressions and extracted D and E parameters for [Fe(EDTA)]$^-$ and transferrin solely from X- and Q-band EPR [50]. With modern EPR software, it is possible to simulate such signals conveniently [51], but the zfs in these systems is of relatively low magnitude ($|D| < 1$ cm^{-1}).

Case studies of HFEPR applied to bioinorganically relevant systems

We provide here, for each of the major mononuclear spin systems ($1/2 < S \leq 5/2$), examples of the application of

HFEPR in metalloproteins or model compounds of bioinorganic relevance. Selected examples of dinuclear systems are also provided. More exotic spin systems are encountered in the molecular magnetism area, and those cases are reviewed elsewhere [35, 52].

$S = 1$ systems

Moderate-magnitude zfs: V(III)

A bioinorganically relevant example of an $S = 1$ system with moderate zfs is a series of aminocarboxylate complexes of V(III), which were studied in frozen aqueous solution [53]. These systems are of interest not because of the importance of this ligand type but due to the potential application of V(III) as an insulin mimetic [54]. Analysis of the field-frequency dependence of the HFEPR spectra allowed the spin Hamiltonian parameters to be determined; e.g., for powder $Na[V(trdta)]\cdot 3H_2O$: $|D| = 5.60\ cm^{-1}$, $|E| = 0.85\ cm^{-1}$, $g = 1.95$. The combination of HFEPR data with crystal structures, electronic absorption spectra, and ligand-field theory (LFT) allowed the relationship between the geometrical and electronic structures to be elucidated for these complexes.

Large-magnitude zfs: Fe(IV) with a triplet ground state

Intense interest has been exhibited over the past two decades in high-oxidation-state iron complexes, as these are invoked as intermediates in both heme and non-heme Fe enzymes [40]. Specifically, complexes of oxoiron(IV) have been prepared as models for non-heme enzymes. Two such complexes have been investigated by HFEPR in the solid state [55]. Here, the zfs is at the upper end of what can be currently measured by HFEPR; a value of $D = +27\ cm^{-1}$ was determined for $[FeO(TMC)(CH_3CN)](CF_3SO_3)_2$, where TMC is tetramethylcyclam. The zfs in these complexes had previously been determined by magnetic (variable external field and variable temperature, VT-VH) Mössbauer spectroscopy, which was in agreement with HFEPR. This may beg the question of why HFEPR is needed. A zero-order answer is that it is always desirable to corroborate one, relatively nontrivial, spectroscopic technique with another (note that zero-field Mössbauer cannot provide this information). A first-order answer is that HFEPR provides information not obtainable from magnetic Mössbauer, namely the g values, and a high-precision measurement of the rhombicity (see also the "$S = 2$ in a magnetic field" section). Such information is of great benefit to computational studies that aim to relate subtleties of electronic structure with reactivity [56].

Other bioinorganically related systems: Ni(II)

A common example of $S = 1$ is six-coordinate (approximately octahedral) Ni(II). This is a classic case of EPR silence, as evidenced by the nomenclature MCR_{silent} for the resting state of methyl-coenzyme M reductase (MCR), which contains Ni(II) in a tetrapyrrole-like (hydrocorphin) cofactor [57]. Sadly, such enzyme forms are yet to be investigated by HFEPR, but Ni(II) in amino acid complexes has been, and quite successfully [58, 59]. Ni(II) complexes of this general type are relevant to Ni trafficking in biology [60] and some of them have been tested for antimicrobial activity. Density functional theory (DFT) was used to understand their zfs.

Four-coordinate (approximately tetrahedral) Ni(II) is another example of an EPR-silent system that is amenable to HFEPR. Thus far, we have refrained from inflicting an actual HFEPR spectrum on the reader; however, this type of complex presents a good opportunity. This is demonstrated in Fig. 7, which presents the HFEPR spectrum of $Tp^{tBu}Ni(NCS)$, where Tp^{tBu} is the hydridotris(3-*t*-butylpyrazol-1-yl)borate anion. The trispyrazolylborate or "scorpionate" ligand $Tp^{R,R'}$, and its many other variants, is used extensively in inorganic chemistry, including as a platform for many bioinorganic model compounds [61, 62].

What is notable in this spectrum is the intense B_{min} feature at ca. 2 T, the origin of which is discussed above in the section "$S = 1$ in a magnetic field," and which is a signature of a triplet state. Its intensity belies the common knowledge of forbidden spin transitions (since it is nominally a $\Delta M_S = \pm 2$ resonance); however, its isotropic behavior is what makes it so intense in randomly oriented systems only (such as powders). Figure 7 also illustrates an important advantage of HFEPR over conventional versions of the technique: its ability to determine the sign of D, in this particular case demonstrating that it is positive. The difference between the two choices of sign is more striking in cases that are shown subsequently.

$S = 3/2$ systems

There are many examples of $S = 3/2$ among the early transition metal ions (e.g., V(II), Cr(III), both $3d^3$), but these are generally not biologically relevant. Mo(III) has proven to be important in dinitrogen activation, but with the required supporting ligands it has an $S = 1/2$ ground state and is successfully studied by conventional EPR [63]. Mn(IV) ($3d^3$), on the other hand, does have biological relevance, albeit often as part of di- or polynuclear centers, such as in Mn catalase [64] and the photosystem II (PSII) oxygen-evolving complex (OEC) [65], and these can be fruitfully studied by conventional EPR (and ENDOR) [66].

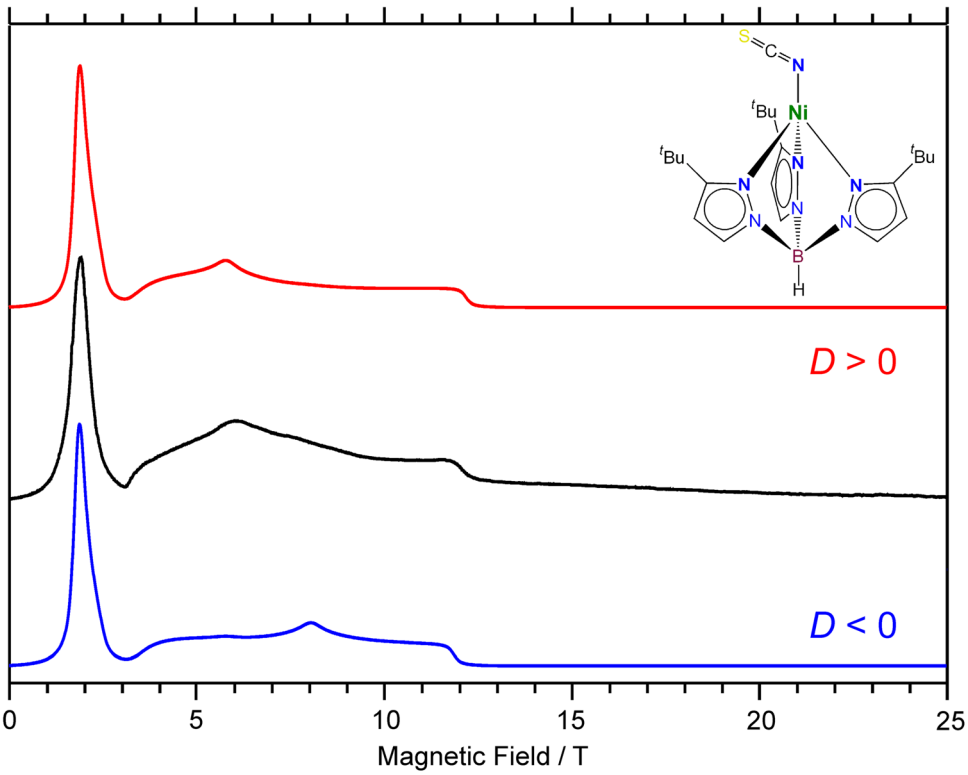

Fig. 7 HFEPR powder spectrum of [$Tp^{tBu}Ni^{II}$(NCS)] (structure shown in the *inset*; *t*Bu = *tert*-butyl, –$C(CH_3)_3$) recorded at 231.0 GHz and 4.2 K (*black trace*) using optical modulation, which gives an absorption lineshape. Simulations use the following spin Hamiltonian parameters: $S = 1$, $|D| = 5.42\ cm^{-1}$, $|E| = 1.12\ cm^{-1}$, $g = [2.15, 2.15, 2.30]$ (*color traces*). *Red trace* was created using positive zfs parameters, and the *blue trace* using negative parameters. It can be seen that the former case fits the experimental signal intensities better

An application of HFEPR to a mononuclear Mn(IV) complex is described in a fairly recent work by Duboc and Collomb [67].

HFEPR-accessible zfs: Co(II) in an approximately tetrahedral geometry

Among the late transition metal ions, Co(II) ($3d^7$) is extremely important, as it has long been used as a spectroscopically active replacement for Zn(II)—a truly EPR-silent ion, as well as one that is largely useless for electronic spectroscopy [68, 69]. Co-substituted Zn proteins are ripe for investigation by HFEPR, but this is yet to be done successfully to our knowledge. In a study of an Fe(III) system (see the section "Moderate zfs: non-heme Fe(III)"), Groenen and co-workers also investigated a biological Co(II) system, Co(II)-substituted desulforedoxin (Fe(II) replaced by Co(II)) and noted that "unfortunately no spectrum of Co(II)–desulforedoxin could be observed in cw at J-band [275 GHz]" [70]. Perhaps Co(II) with an S4 donor set is not amenable to HFEPR; we have had good success with model compounds with N4 donor sets, so it may be that Co(II)-substituted proteins with N and/or O donor coordination offer a better chance of success.

Specifically, we have studied a series of scorpionate complexes of Co(II) of general formula $Tp^{R,R'}CoL$, where $Tp^{R,R'}$ = hydridotris(3-*R*-5-*R*′-trispyrazol-1-yl)borate and L = halide and pseudohalide ligands [71]. Despite the similarity among structures and donor sets, the zfs parameters for these complexes are highly variable. Quantum chemical calculations on Co(II) scorpionates are in progress [72]. Figure 8 presents the HFEPR spectrum of $Tp^{tBu,Np}CoN_3$, where $Tp^{tBu,Np}$ is the hydridotris(3-*t*-butyl-5-neopentylpyrazol-1-yl)borate anion. Of particular significance is the observation of the inter-Kramers transitions at a sufficiently high frequency (in this case, 406 GHz), which allows one to directly extract zfs parameters. Figure 8 again illustrates, more dramatically than in Fig. 7, the ability of HFEPR to determine the sign of *D*, in this particular case demonstrating that it is positive.

HFEPR-inaccessible zfs: Co(II) in an approximately octahedral geometry

This is another important geometry of Co(II), and not only for coordination complexes [73]—it has also recently become relevant in bioinorganic chemistry. There are many metalloenzymes that contain carboxylate-bridged dinuclear sites in which at least one site has a six-coordinate geometry [38–40]. It now appears that Co(II) may be relevant among the possible M(II) ions in such enzymes [74–77]. Examples are the ubiquitous N-terminal methionine aminopeptidase (MetAP), an aminopeptidase found in *Aeromonas proteolytica* and a glycerophosphodiesterase from *Enterobacter aerogenes* (GpdQ) [75]. Although it is not necessarily the case that Co(II) is the native metal ion,

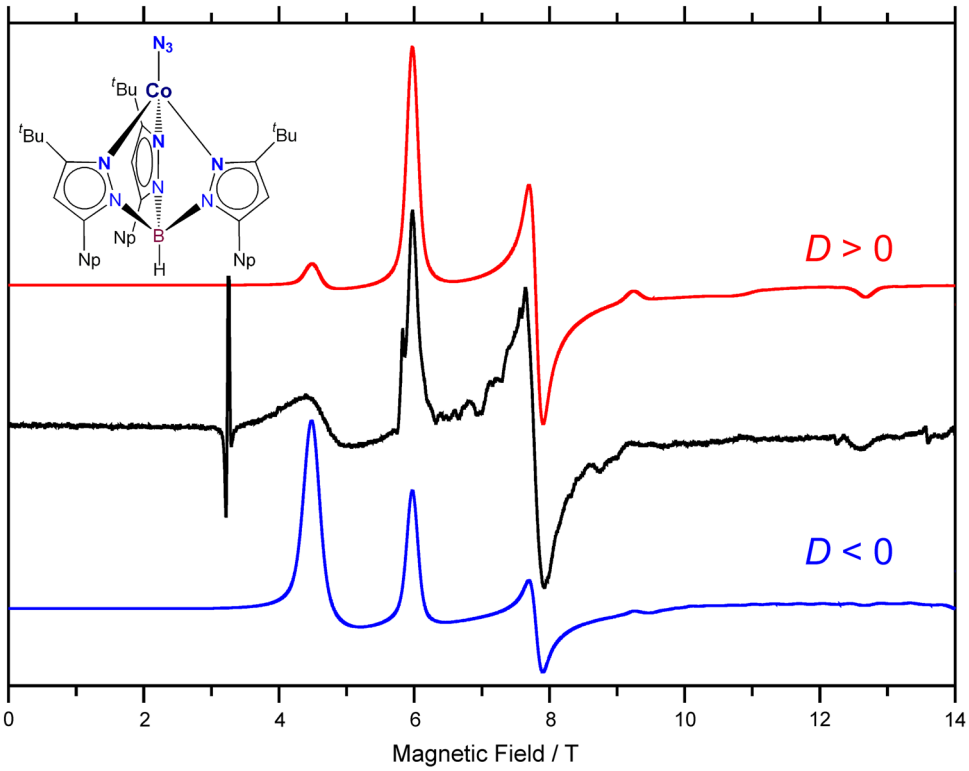

Fig. 8 HFEPR powder spectrum of $[Tp^{tBu,Np}Co^{II}N_3]$ (structure shown in the *inset*; tBu = *tert*-butyl, Np = neopentyl, $-CH_2C(CH_3)_3$) recorded at 406.4 GHz and 10 K (*black trace*) with simulations using the following spin Hamiltonian parameters: $S = 3/2$, $|D| = 11.27\ cm^{-1}$, $|E| = 0.80\ cm^{-1}$, $g = [2.265, 2.330, 2.205]$ (*color traces*). *Red trace* was created using positive zfs parameters, and the *blue trace* using negative parameters. It can be seen that the former case fits the experimental signal intensities better. The peaks at 4.5 and 12.6 T are inter-Kramers transitions, while those at 6 and 7.7 T are intra-Kramers. The sharp resonance at 3.2 T in the experimental spectrum is an impurity induced during sample preparation (grinding with *n*-eicosane, which may have led to decomposition reactions involving the azido group), and is not reproduced in the simulation. The apparent structure between the resonances at 6 and 7.7 T is due to an imperfect powder pattern, and is not simulated either

it is enzymatically effective, and Co(II)-substituted MetAP and GpdQ have been extensively investigated by MCD spectroscopy [75, 78].

For EPR, the difficulty with six-coordinate Co(II) is its orbital degeneracy. In O_h symmetry, the ground state is $^4T_{1g}$, which is lowered either by the Jahn–Teller effect or, more relevantly in biological systems, through ligand inequivalence or structurally induced distortion. If there is axial compression then the ground state is ^4E_g; if there is axial elongation then the ground state is $^4A_{2g}$ (in D_{4h} symmetry; the g subscripts are omitted for D_{2d} and C_{4v}). In the first case, one has an orbitally degenerate ground state, which is anathema to successful HFEPR spectroscopy. We have encountered such systems in $[CoF_6]^{3-}$ (Co(III), $3d^6$) and $CrCp_2$ (Cr(II), $3d^4$, Cp = cyclopentadiene anion), and their HFEPR has been problematic (and is thus unpublished). In the second case, one has an orbitally nondegenerate ground state and HFEPR (as well as conventional EPR) is usually successful. The problem is that the mixing of low-energy excited states leads to large zfs, with the result that only the intra-Kramers signal is seen, providing an EPR spectrum similar to the case described above (see "$S = 3/2$ in a magnetic field") for nitrogenase FeMoco, even at very high frequencies. For example, a study of a model compound for acid phosphatases (another type of di-iron carboxylate-bridged enzyme) in which the Fe(III) site was substituted by Ga(III) and the Fe(II) site by Co(II) showed, even at 635 GHz, such an EPR signal: $\mathbf{g}' = [5.75, 3.60, 2.00]$. Much higher frequencies are required to determine the zfs, such as those that may be achieved using far-IR spectroscopy [79].

$S = 2$ systems

This represents the spin system that appears to have been most fruitfully investigated by HFEPR. It includes ions of less relevance to bioinorganic chemistry, such as Cr(II) ($3d^4$) [80]. Bioinorganically relevant systems comprise Mn(III) ($3d^4$), Fe(II) ($3d^6$), and Fe(IV) ($3d^4$, which can also have a spin triplet ground state; see the section "Large-magnitude zfs: Fe(IV) with a triplet ground state").

Metalloproteins and model compounds: hemes and porphyrins

A breakthrough in the bioinorganic application of HFEPR was achieved by Hori and co-workers, who reported a HFEPR study of myoglobin reconstituted with Mn(III)-protoporphyrin IX (Mn(III)-Mb) [81]. They were able to determine the full set of spin Hamiltonian parameters for this system, which were similar to those seen for isolated Mn(III) porphyrins. More significantly, they extended this work to deoxy-Mb and deoxy-Hb, so that the native Fe(II) system has now been studied [82]. Given the large number of heme proteins (enzymes) available, this represents a promising area for further applications of HFEPR.

A large number of Mn(III)-containing porphyrins, and related complexes such as corroles, have been studied by HFEPR [33, 83, 84]. The zfs of such systems is in a "sweet spot" (i.e., ideal frequency range) for HFEPR spectrometers. We therefore cannot resist showing in Fig. 9 a spectrum of such a system [Mn(tpfc)], tpfc = 5,10,15-tris(pentafluorophenyl)corrole trianion [85], recorded in benzene solution. Note that a quintet powder spectrum is not readily recognizable; it looks nothing like that of a "typical" triplet pattern, such as those seen for V(III) or Ni(II) [86, 87], even with similar-magnitude zfs. The assignment of the particular resonances is only possible via simulations, such as those shown in Fig. 5.

Metalloproteins and model compounds: iron-sulfur proteins

Another important class of metalloproteins is the iron-sulfur proteins. This is a large class containing many members that have states that are observable by conventional EPR. Indeed, EPR was crucial in the discovery of FeS proteins by Beinert [88]. Thus far, only the simplest of the FeS centers encountered in biology has been successfully investigated by HFEPR, namely the reduced rubredoxin (Rd-red) center $[Fe(cys)_4]^{2-}$. This center was studied first as a model complex, $(PPh_4)_2[Fe(S(C_6H_5)_4]$ [89], which had been investigated much earlier using both VTVH-Mössbauer and far-IR spectroscopy. The spin Hamiltonian parameters for this complex were determined as: $D = +5.84\ cm^{-1}$, $E = +1.42\ cm^{-1}$, $g_x = g_y = 2.08$, $g_z = 2.00$. The agreement in zfs was good with far-IR ($D = +5.98\ cm^{-1}$, $E = +1.42\ cm^{-1}$), but not with Mössbauer ($|D| = 7.55\ cm^{-1}$). We believe that this discrepancy is due to the relatively high rhombicity of this complex, $|E/D| = 0.24$. Techniques that rely on the VTVH methodology (such as Mössbauer, MCD, and magnetometry) but do not observe resonant transitions (as in (HF)EPR) have difficulty in distinguishing different contributions to zfs effects.

More recently, an authentic Rd-red protein was studied using HFEPR by Barra and co-workers in Grenoble [90].

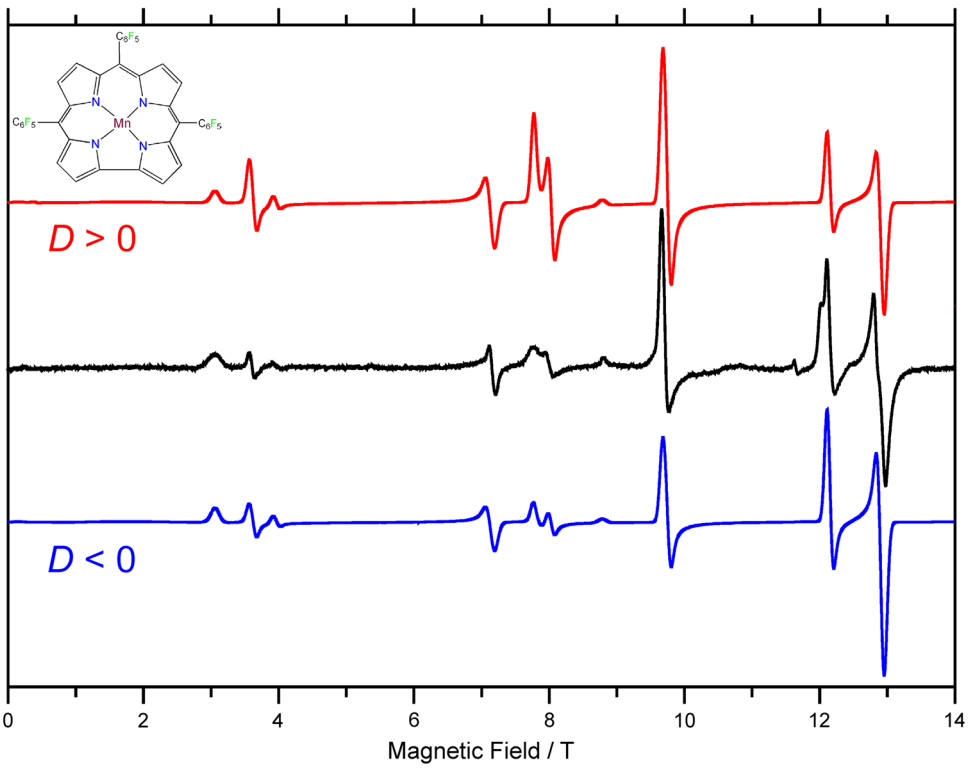

Fig. 9 HFEPR spectrum of a 2 mM solution of $[Mn^{III}(tpfc)]$ (structure shown in the *inset*; tpfc = 5,10,15-tris(pentafluorophenyl)corrole trianion) in benzene recorded at 326.4 GHz and 30 K (*black trace*) with simulations using the following spin Hamiltonian parameters: $S = 2$, $|D| = 2.67\ cm^{-1}$, $|E| = 0.023\ cm^{-1}$, $g = [1.99, 1.99, 2.00]$ (*color traces*). *Red trace* was created using positive zfs parameters, and the *blue trace* using negative parameters. It can be seen that the latter case fits the experimental signal intensities better

This was the protein from the hyperthermophile *Pyrococcus abyssi* expressed in *Escherichia coli* (certain mutations were needed to achieve protein expression, but these do not affect the FeS center) [90]. Similar results to those seen for the Rd model compound were obtained. The spin Hamiltonian parameters for the FeS center were extracted by multi-frequency (190, 230, 285, 345, 380 GHz) HFEPR to give a highly rhombic zfs, similar to the model compound: $D = +4.8(2)$ cm^{-1}, $E = +1.2(5)$ cm^{-1}, $g_x = g_y = 2.1$, $g_z = 2.0$. VTVH-Mössbauer had previously given $D = +5.6(5)$ cm^{-1}, $E = +1.3(1)$ cm^{-1}. The discrepancy here is less than that seen for the model compound, but it still suggests that fitting a complete field-frequency HFEPR data set is the optimal method of studying such a system, whenever possible.

Other possibilities

Obviously, the many non-heme enzymes (which have been studied by techniques such as MCD [39]) and their model complexes [91] are potential candidates for HFEPR in their Fe(II) forms, even, we believe, in cases where VTVH-Mössbauer has been performed. Another, related, opportunity is to study these enzymes in their active $S = 2$ Fe(IV) forms. Model complexes with this spin ground state have recently been reported [92] and likewise present an opportunity for HFEPR.

Coordination complexes of Mn(III) have been studied by HFEPR [33, 35, 93] and analyzed by the latest computational methods [94]. From a bioinorganic perspective, a metalloenzyme such as Mn superoxide dismutase (MnSOD), which contains Mn(III) in the oxidized form, might be a good candidate for HFEPR. The low-field EPR signal (see "$S = 2$ in a magnetic field") of MnSOD has been previously studied by parallel-mode X-band EPR [48]. A more recent and very intriguing system is the di-Mn class 1b ribonucleotide reductase from *E. coli* [95]. This has been investigated by conventional EPR in [Mn(III)$_2$-Y$^\bullet$], where Y$^\bullet$ is a catalytically essential tyrosyl radical, and in the [Mn(III)Mn(IV)] form, which has a net $S = 1/2$ ground state [96]. An enzyme form containing a magnetically isolated Mn(III) (whether alone or with a diamagnetic ion) would possess great potential for HFEPR.

$S = 5/2$ systems

Because of the intrinsically smaller zfs [32] of this spin system ($^6A_{1g}$ ground state in O_h symmetry, and always the totally symmetric representation in whatever point group symmetry), HFEPR is not always necessary. Nevertheless, there are cases where the zfs can be significant, and even when not, the technique can give valuable information.

Small zfs: Mn(II)

Six-coordinate Mn(II) gives one of the most ubiquitous EPR signals, which is often observable, especially at higher frequencies from adventitious sources. There are, however, enzymes containing mononuclear Mn(II) that have been studied fruitfully by HFEPR. These include reduced MnSOD [97–100], and oxalate oxidase (OxOx)/oxalate decarboxylase (OxDC) [101–103], which exhibited $|D| \leq 0.4$ cm^{-1}, as helpfully summarized by Tabares et al. [101]. Changes in zfs as a function of biochemically important events, such as pH changes and substrate binding, could be monitored by HFEPR [101].

Moderate zfs: non-heme Fe(III)

In the case of Fe(III), coordination complexes with biologically relevant ligands such as aminocarboxylates and others have been studied by HFEPR in aqueous solution [104, 105]. This suggests that metalloenzymes, such as non-heme Fe enzymes in their Fe(III) form, are good candidates for HFEPR.

The oxidized form of a rubredoxin (Rd-ox, $[Fe(cys)_4]^-$) center, specifically the desulforedoxin from *Desulfovibrio gigas* (expressed in *E. coli*), has been studied by HFEPR at 275 GHz (10 mM aqueous solution) to give $D = +2.40$ cm^{-1}, $E = +0.18$ cm^{-1}, $g_x = g_y = 2.020$, $g_z = 2.025$ [70, 104]. These precisely determined values can be compared to those from a combination of X-band EPR (which gives signals at $g' = 8.82$, 4.2, 1.8 from the $\langle S, M_S| = \langle 5/2, \pm 1/2|$ ground state and $g' = 5.82$ from the $\langle S, M_S| = \langle 5/2, \pm 3/2|$ excited state) and Mössbauer, which gave $|D| \approx 2$ cm^{-1}, $|E| \approx 0.16$ cm^{-1}. This is not a serious difference, but nevertheless serves to document the superiority of HFEPR in obtaining zfs parameters, when feasible.

Large zfs: heme Fe(III)

Heme proteins (enzymes) are also relevant. In this case, the zfs can be too large for direct extraction by HFEPR. An interesting study by van Kan et al. [106] used the full panoply of EPR frequencies available at the time (1 (L-band), 3 (S-band), 9 (X-band), 35 (Q-band), 130 (D-band), 195 (looking for a letter) and 285 (J-band) GHz) to monitor the $g'_\perp \approx 6$ band of met-Mb. The resonant field/frequency dependence of $g'_\perp$ allows an estimate of the zfs ($D \approx +10$ cm^{-1}) because of second-order effects: at higher fields there is increased mixing in of the $\langle 5/2, \pm 3/2|$ (and, to a much lesser extent, $\langle 5/2, \pm 5/2|$) excited states as the increasing Zeeman effect brings these states closer in energy to the $\langle 5/2, \pm 1/2|$ ground state. However, there was no direct

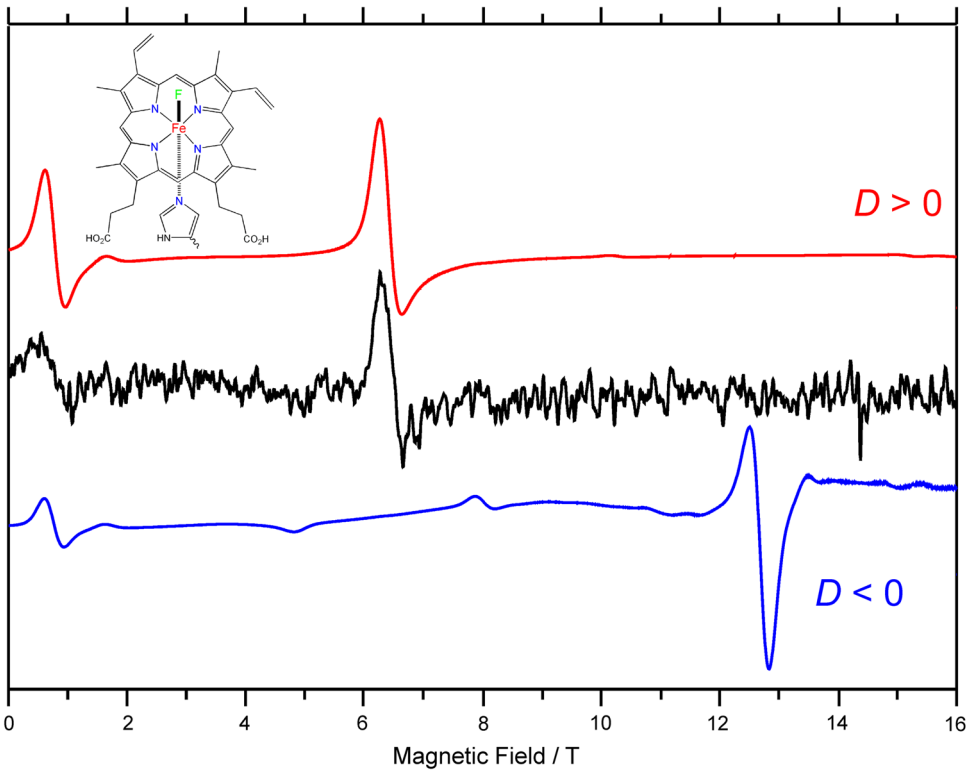

Fig. 10 HFEPR spectrum of fluorometmyoglobin in aqueous pH 6 buffer, prepared as described elsewhere [49]. The *inset* shows the active site, consisting of ferric heme with proximal histidine and distal fluorido ligand ([Fe^{III}(PPIX)(im)F], PPIX = protoporphyrin IX, im = imidazole from histidine). The data were recorded at 396 GHz and 4.2 K in a resistive magnet (*black trace*) with simulations using the following spin Hamiltonian parameters: $S = 5/2$, $|D| = 5.85\ \text{cm}^{-1}$, $E = 0$, $g = 2.00$ (*color traces*). *Red trace* was created using positive D, and the blue trace using negative D. It can be seen that the former case better fits the experimental signal intensities. The resonance at ca. 1 T is an inter-Kramers transition; that at ca. 6.5 T is an intra-Kramers transition ($g_{\text{eff}} = 4.4$) which is observable at low frequencies as well at roughly the same effective g value [106]

observation of an $\langle 5/2, \pm 1/2| \rightarrow \langle 5/2, \pm 3/2|$ inter-Kramers transition, in contrast to the case for certain Co(II) systems [71]. We have also been unable to see such a transition in met-Mb, even at higher frequencies. However, replacing the axial aqua ligand with a fluorido ligand reduced the zfs such that the inter-Kramers transition can be observed and the zfs parameters obtained directly in met-Mb-F. This is shown in Fig. 10. Very recently, HFEPR using coherent synchrotron radiation in the THz region was applied to met-Mb and met-Mb-F. This technique allowed observation of the inter-Kramers transition in both systems and gave for met-Mb-F: $D = +5.0(1)\ \text{cm}^{-1}$, $g_{\perp} = 2.025(5)$ ($g_{\|}$ set at 2.00; pH 7) [107]. This D value differs significantly from that derived from HFEPR ($+5.85\ \text{cm}^{-1}$; Fig. 10) and ENDOR ($+6.1(1)\ \text{cm}^{-1}$; see "*S* = 5/2 in a magnetic field"); both at pH 6 and on samples prepared in the same laboratory [49]. Note that a pioneering far-IR study gave $D = +5.94\ \text{cm}^{-1}$ [108]. Thus, the take-home message regarding met-Mb-F, and likely other metalloproteins, may be that identical samples should be studied to achieve a controlled comparison among techniques.

Dinuclear systems

The simplest such transition metal system is di-Cu(II), by virtue of having a total of only two unpaired electrons. This species has biological relevance, as in dinuclear Cu enzymes such as those with type 3 centers (tyrosinase) and even those with higher nuclearity (Cu_Z) [109] and perhaps pMMO [110]. Antiferromagnetic coupling ($S_{\text{total}} = S_1 - S_2 = 1/2 - 1/2 = 0$) leads to a diamagnetic singlet ground state, but even when this is the case, higher temperatures readily allow access to the paramagnetic triplet ($S_{\text{total}} = S_1 + S_2 = 1/2 + 1/2 = 1$) excited state for detection by EPR. Examples include a variety of coordination complexes with carboxylato and pyrazolyl or other ligands [111–115], in which the zfs of the excited triplet state can be measured.

Figure 11 presents the HFEPR spectrum of one such di-Cu(II) complex, $[Cu_2(H_2tea)_2(2\text{-nitrobenzoate})_2]_2(H_2O)_3$ (where H_2tea = monodeprotonated triethanolamine) [115]. In this case, as clearly shown by magnetometry, the coupling is strongly ferromagnetic ($J = -100\ \text{cm}^{-1}$; $\mathcal{H}_{\text{exch}} = J\hat{S}_1 \cdot \hat{S}_2$), so that the triplet is the ground state and is best

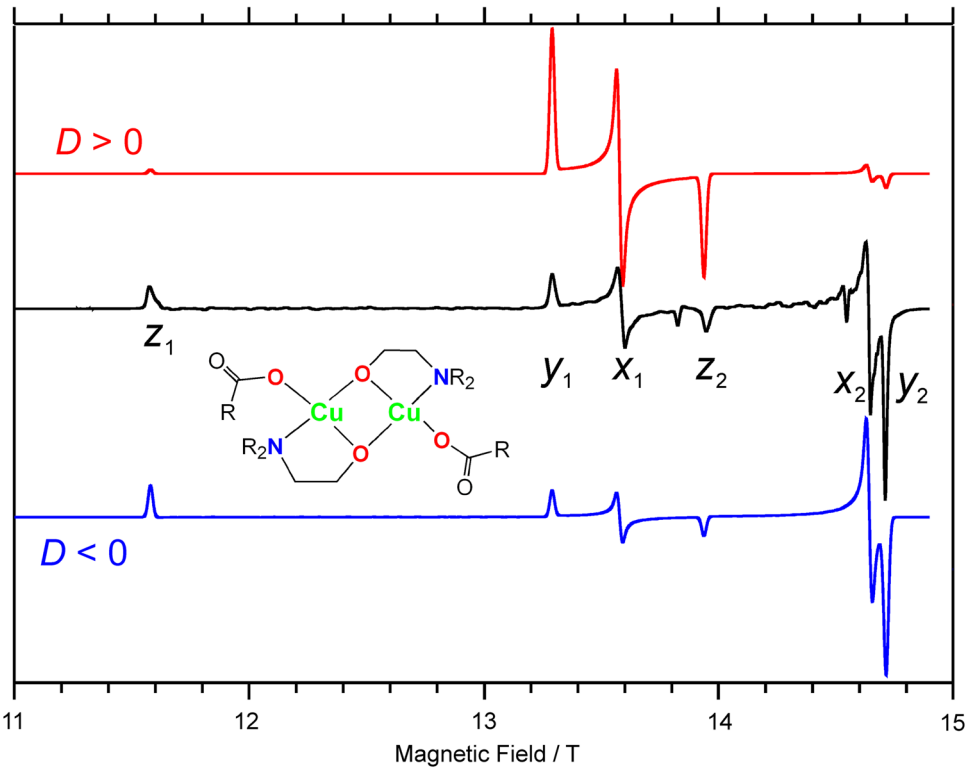

Fig. 11 HFEPR powder spectrum of $[CuII_2(H_2tea)_2(2\text{-nitrobenzoate})_2]_2(H_2O)_3$ (where H_2tea = monodeprotonated triethanolamine; a simplified structure is shown in the *inset*) recorded at 406.4 GHz and 10 K with simulations using the following spin Hamiltonian parameters: $S = 1$, $|D| = 1.042\ cm^{-1}$, $|E| = 0.0075\ cm^{-1}$, $g = [2.056, 2.045, 2.320]$ (*color traces*) [115]. *Red trace* was created using positive zfs parameters, and the blue trace using negative parameters. It can be seen that the latter case better fits the experimental signal intensities. Labeling of triplet transitions is also provided

observed at low temperatures. In this well-resolved triplet spectrum, the transitions are identified using standard nomenclature [7].

Other dinuclear systems can be studied by HFEPR, such as an Fe(II)–Fe(III) complex in which the ferromagnetically coupled state ($S_{total} = S_1 + S_2 = 5/2 + 2 = 9/2$) is the ground state [31]. This study of a model compound was done a number of years ago, but it demonstrates the potential for HFEPR to investigate metalloproteins with the $S = 9/2$ ground state, as found in mutant forms of *Clostridium pasteurianum* 2Fe ferredoxin (Fd) for instance [30]. Obviously, the antiferromagnetic situation ($S_{total} = S_1 - S_2 = 5/2 - 2 = 1/2$) commonly found in "normal" 2Fe-Fds and in di-iron-oxo proteins such as hemerythrin (Hr) and sMMO is one for which conventional EPR is fruitful [116–119]. In principle, any of these di-iron oxo proteins could also be studied in their $Fe(II)_2$ or $Fe(III)_2$ forms, although it might require higher temperatures to observe transitions among the non-singlet excited states. Coordination complexes with di-Fe(II) and di-Mn(II) have already been successfully studied by HFEPR, allowing the extraction of single ion zfs and exchange coupling parameters [111]. Di-Mn(II) is relevant to metalloenzymes such as arginase [120]. HFEPR of di- and polynuclear species has been popular in the molecular magnetism area for some time [35, 52], and deserves to be applied more extensively to bioinorganic analogs.

Relationship between spin Hamiltonian parameters and bonding information

The earlier section "Case studies of HFEPR applied to bioinorganically relevant systems" demonstrated the wide range of bioinorganically relevant systems that have been (or perhaps should be) examined by HFEPR, and the ability of this technique to extract spin Hamiltonian parameters, i.e., zfs splitting and g values. However, a question naturally arises: so what? What does one do with these parameters? If would be nice if, say, D values were like chemical shifts in ^1H NMR and could be easily correlated with chemical structure. This is unfortunately not the case. In the first place, each d^n system and, to a great extent, each coordination symmetry thereof must be treated as a separate case. This is not even taking into account the difference among metal ions with the same d^n count and the potentially substantial contribution to zfs from SOC involving highly covalent ligands [121, 122]. This is not to say that zfs parameters for related complexes are random; it is possible to make some generalization from a series of

complexes, such as the Co(II) monoscorpionates [71]. What is necessary for quantitative analysis is a complete quantum chemistry study, using ab initio methods if possible, of a given system in order to extract the origin of the experimentally observed zfs [32, 94, 121, 123–126]. The same approach is needed for g values [127], from EPR at whatever frequency/field, and hyperfine coupling constants [128], which are best extracted experimentally by lower frequency/field EPR. As can be seen from the references cited, which are far from complete, the group of F. Neese (Max Planck Institute for Chemical Energy Conversion, Mülheim/Ruhr, Germany) is the dominant force in this area, to some extent due to his spectroscopically oriented, versatile, and free software package ORCA [129]. The potential pitfalls in using quantum chemistry programs, such as the deficiencies of DFT in analyzing $S > 1/2$ complexes, are beyond the scope of this minireview, but when properly applied these theoretical methods are extremely powerful [25, 124, 130]. We believe that more classical methods, namely LFT programs such as DDN (available from J. Telser) and Ligfield (by J. Bendix, Copenhagen University, Denmark) [27] are also helpful, and LFT has indeed been very fruitfully combined with quantum chemistry methods in recent studies [125, 126].

Case study of tetragonally distorted five-coordinate or six-coordinate high-spin $d^{4,6}$

The above discussion passes the buck to the quantum chemistry experts, and this is the current situation. However, it is still possible to use simple examples to give a feel for the physical origins of zfs and its relation to geometry and bonding. The first such example, tetragonally distorted high-spin d^4, is one that has been extensively studied, as it is relevant to Mn(III) in porphyrins [131]. Because of the relation between electron and hole, this is also relevant to tetragonally distorted high-spin d^6, as in Fe(II) in similar coordination environments.

As free ions, the ground-state term of $d^{4,6}$ is ^5D—the only term with $S = 2$. In an octahedral ligand field, this term splits into a ^5E_g ground state ($t_2^3e^1$ in a strong field representation) and a $^5T_{2g}$ excited state ($t_2^2e^2$) for d^4, with the reverse order in energy for d^6 (respectively, $t_2^4e^2$ and $t_2^3e^3$). With tetragonal elongation (i.e., along a C_4 axis), the ^5E_g state splits into $^5A_1$ and $^5B_1$ (in C_{4v}; add g subscripts for D_{4h}) and the $^5T_{2g}$ state splits into $^5B_2$ and ^5E (g subscripts for D_{4h}). The $^5A_1$ state corresponds to the hole (for d^4) or electron (for d^6) in the d_{z^2} orbital, $^5B_1$ to the hole/electron in the $d_{x^2-y^2}$ orbital, $^5B_2$ to the hole/electron in the d_{xy} orbital, and ^5E to the hole/electron in the degenerate $d_{xy,\ yz}$ orbitals. The orbitals can typically be ordered in terms of energy as follows: $d_{xy}, d_{xz,yz}, d_{z^2}, d_{x^2-y^2}$, so that the ground state is $^5B_1$ for d^4 ($^5B_2$ for d^6). The electron spins can then be added to give the various states; we use only d^4 because there are fewer electrons, simplifying the writing. The $^5B_1$ ground state can be written as follows, using Slater determinants:

$$^5B_1(M_S = +2) = \left[d_{xy}^+ d_{xz}^+ d_{yz}^+ d_{z^2}^+\right],$$

$$^5B_1(M_S = +1) = \frac{1}{\sqrt{4}}\left[d_{xy}^+ d_{xz}^+ d_{yz}^+ d_{z^2}^- + d_{xy}^+ d_{xz}^+ d_{yz}^- d_{z^2}^+ + d_{xy}^+ d_{xz}^- d_{yz}^+ d_{z^2}^+ + d_{xy}^- d_{xz}^+ d_{yz}^+ d_{z^2}^+\right],$$

$$^5B_1(M_S = 0) = \frac{1}{\sqrt{6}}\left[\begin{array}{l} d_{xy}^+ d_{xz}^+ d_{yz}^- d_{z^2}^- + d_{xy}^+ d_{xz}^- d_{yz}^+ d_{z^2}^- + d_{xy}^- d_{xz}^+ d_{yz}^+ d_{z^2}^- \\ + d_{xy}^- d_{xz}^- d_{yz}^+ d_{z^2}^+ + d_{xy}^- d_{xz}^+ d_{yz}^- d_{z^2}^+ + d_{xy}^+ d_{xz}^- d_{yz}^- d_{z^2}^+ \end{array}\right].$$

The excited states are written analogously (only $M_S = +2$ is given), in ascending order of energy, as

$$^5A_1(M_S = +2) = \left[d_{xy}^+ d_{xz}^+ d_{yz}^+ d_{x^2-y^2}^+\right],$$

$$^5E_a(M_S = +2) = \left[d_{xy}^+ d_{xz}^+ d_{z^2}^+ d_{x^2-y^2}^+\right],$$

$$^5E_b(M_S = +2) = \left[d_{xy}^+ d_{yz}^+ d_{z^2}^+ d_{x^2-y^2}^+\right],$$

$$^5B_2(M_S = +2) = \left[d_{xz}^+ d_{yz}^+ d_{z^2}^+ d_{x^2-y^2}^+\right].$$

How does this situation lead to zfs? We have to apply SOC, in this case using the form for single electrons, summed over all of the electrons present:

$$\mathcal{H}_{LS} = \zeta \sum_i (\hat{l}_i \cdot \hat{s}_i),$$

where ζ is the single-electron SOC constant, which is quite variable depending on the metal ion [27]. The effect of $\mathcal{H}_{LS}$ on the d orbitals is given in many places, e.g., Table III in McGarvey [132]. We need to find which spin quintet excited states can interact via SOC with the ground state. If this interaction differs in energy for the different M_S states within a given orbital state, then zfs results.

Let us now see how SOC functions in this case. First, consider the possible effect of the $^5A_1$ excited state. To have a nonzero matrix element, one must convert $d_{x^2-y^2}$

into d_{z^2}. There is no operator that does this, so all matrix elements $\langle {}^5B_1 | H_{\rm LS} | {}^5A_1 \rangle = 0$, and thus the effect of this excited state on zfs, $D_{A_1} = 0$. However, the $\hat{l}_z$ operator connects the $d_{x^2-y^2}$ and d_{xy} orbitals, so there are potentially matrix elements $\langle {}^5B_1 | H_{\rm LS} | {}^5B_2 \rangle \neq 0$, and the ${}^5B_2$ excited state can thus contribute to zfs. Evaluating these for each $M_{\rm S}$ level gives the following:

$$\langle {}^5B_1(2) | H_{\rm LS} | {}^5B_2(2) \rangle = -i\zeta,$$
$$\langle {}^5B_1(1) | H_{\rm LS} | {}^5B_2(1) \rangle = -\frac{i}{2}\zeta,$$
$$\langle {}^5B_1(0) | H_{\rm LS} | {}^5B_2(0) \rangle = 0.$$

The last of these is zero because the $\hat{s}_z$ operator gives three $m_{\rm s} = +\frac{1}{2}$ and three $m_{\rm s} = -\frac{1}{2}$, so all of the terms cancel out. The application of second-order perturbation theory gives the following effects of these matrix elements:

$$\Delta E_{B_2}(2) = -\frac{\zeta^2}{\Delta E({}^5B_2 - {}^5B_1)},$$
$$\Delta E_{B_2}(1) = -\frac{1}{4}\frac{\zeta^2}{\Delta E({}^5B_2 - {}^5B_1)},$$
$$\Delta E_{B_2}(0) = 0,$$

where $\Delta E({}^5B_2 - {}^5B_1)$ is the energy of that electronic transition (i.e., the energy separation between the d_{xy} and $d_{x^2-y^2}$ orbitals). The $S = 2$ spin Hamiltonian gives the separation between the $M_{\rm S} = \pm 2$ and ± 1 levels as $3D$, and between ± 1 and 0 as D. The above equations show that

$$\Delta E_{B_2}(2) - \Delta E_{B_2}(1) = -\frac{3}{4}\frac{\zeta^2}{\Delta E({}^5B_2 - {}^5B_1)} = 3D_{B_2},$$
$$\Delta E_{B_2}(1) - \Delta E_{B_2}(0) = -\frac{1}{4}\frac{\zeta^2}{\Delta E({}^5B_2 - {}^5B_1)} = D_{B_2},$$

so $D_{{}^5B_2} = -\frac{\zeta}{4}\frac{1}{\Delta E({}^5B_2 - {}^5B_1)}$, which is the same as $D_{{}^5B_2} = -4\lambda^2\frac{1}{\Delta E({}^5B_2 - {}^5B_1)}$ since $\lambda = \frac{\zeta}{4}$.

Because the $\hat{l}_x$ and $\hat{l}_y$ operators respectively convert $d_{x^2-y^2}$ into d_{yz} and d_{xz}, the ${}^5E$ excited state can also contribute to zfs. The calculation is more involved, but analogous to the above. The SOC Hamiltonian applied here respectively involves the $\hat{s}_x$ and $\hat{s}_y$ operators as well, so that a spin flip is required. The nonzero matrix elements are as follows:

$$\left\langle {}^5B_1(\pm 1) | H_{LS} | {}^5E_a(\pm 2) \right\rangle = \left\langle {}^5B_1(\pm 2) | H_{LS} | {}^5E_a(\pm 1) \right\rangle = \frac{i}{4}\zeta,$$
$$\left\langle {}^5B_1(\pm 1) | H_{LS} | {}^5E_a(0) \right\rangle = \left\langle {}^5B_1(0) | H_{LS} | {}^5E_a(\pm 1) \right\rangle = \sqrt{\frac{3}{2}}\frac{i}{4}\zeta;$$
$$\left\langle {}^5B_1(\pm 1) | H_{LS} | {}^5E_b(\pm 2) \right\rangle = \left\langle {}^5B_1(\pm 2) | H_{LS} | {}^5E_b(\pm 1) \right\rangle = -\frac{1}{4}\zeta,$$
$$\left\langle {}^5B_1(\pm 1) | H_{LS} | {}^5E_b(0) \right\rangle = \left\langle {}^5B_1(0) | H_{LS} | {}^5E_b(\pm 1) \right\rangle = -\sqrt{\frac{3}{2}}\frac{1}{4}\zeta.$$

The application of second order perturbation theory gives the following effects of these matrix elements:

$$\Delta E_{{}^5E}(2) = -\frac{1}{16}\frac{2\zeta^2}{\Delta E({}^5E - {}^5B_1)},$$
$$\Delta E_{{}^5E}(1) = -\frac{1}{16}\frac{5\zeta^2}{\Delta E({}^5E - {}^5B_1)},$$
$$\Delta E_{{}^5E}(0) = -\frac{1}{16}\frac{6\zeta^2}{\Delta E({}^5E - {}^5B_1)},$$

with the result that:

$$\Delta E_{{}^5E}(2) - \Delta E_{{}^5E}(1) = -\frac{3}{16}\frac{\zeta^2}{\Delta E({}^5E - {}^5B_1)} = 3D_{{}^5E},$$
$$\Delta E_{{}^5E}(1) - \Delta E_{{}^5E}(0) = -\frac{1}{16}\frac{\zeta^2}{\Delta E({}^5E - {}^5B_1)} = D_{{}^5E},$$

so that the contribution to zfs from the ^{5}E excited state is: $D_{{}^5E} = +\frac{\zeta^2}{16}\frac{1}{\Delta E({}^5E - {}^5B_1)} = +\lambda^2\frac{1}{\Delta E({}^5E - {}^5B_1)}$, where the denominator is the appropriate electronic transition energy. Note that $D_{{}^5B_2}$ and $D_{{}^5E}$ are of opposite sign.

The above discussion considered excited states arising only from the ${}^5D$ free ion (i.e., quintet spin states only; 25 microstates). However, there are numerous triplet (135 microstates) and singlet (50 microstates) excited states as well. Most of these are too high in energy to contribute significantly to zfs, but one triplet excited state, ${}^3E$, arising from ${}^3T_{1g}$ in O_h symmetry ($t_2^4e^0$ in strong-field representation; primarily from free-ion ^{3}H), is often accessible in energy. In the bonding description employed here, ${}^3E$ corresponds to (only $M_{\rm S} = +1$ is given)

$${}^3E_{\rm a}(M_{\rm S} = +1) = \left[d_{xy}^+ d_{xz}^+ d_{xz}^- d_{z^2}^+ \right],$$
$${}^3E_{\rm b}(M_{\rm S} = +1) = \left[d_{xy}^+ d_{yz}^+ d_{yz}^- d_{z^2}^+ \right].$$

The contribution of this ${}^3E$ excited state to zfs has been derived in detail elsewhere [131] and corresponds to

$$D_{{}^3E} = -\frac{\zeta^2}{4}\frac{1}{\Delta E({}^3E - {}^5B_1)}.$$

Thus, the observed D value in a tetragonally distorted d^4 complex, such as an Mn(III) porphyrin, contains contributions from at least three excited states (i.e., $D_{\rm total} = D_{{}^5B_2} + D_{{}^5E} + D_{{}^3E}$), requiring knowledge of their energies. Note that only the electronic transition ${}^5B_1 \rightarrow {}^5E$ is both spin-allowed and dipole-allowed in C_{4v} point group symmetry (with x, y polarization); ${}^5B_1 \rightarrow {}^5B_2$ (and ${}^5A_1$) is symmetry forbidden. The energy of the triplet excited state(s) requires knowledge of interelectronic repulsion terms (Racah parameters) and, most of all, one needs to know the value to use for ζ, which is likely reduced from its free-ion value. As a result, methods such

as that described here can provide only an estimate of the value of the zfs, but LFT is useful for gaining an understanding of both the physical origins and significance of this effect, and providing a starting point for ab initio calculations [125], as will be described in the next section.

Case study of trigonally distorted four-coordinate high-spin d^8

As free ions, the ground term of $d^{2,8}$ is ^3F, but there is also a ^3P higher-energy term. In a tetrahedral field, these split into a $^3T_1(F)$ ground state ($e^4t_2^4$ in a strong field representation), and $^3T_2(F)$ ($e^3t_2^5$), $^3A_2(F)$ ($e^2t_2^6$; the ground state for an octahedral d^8 complex), and $^3T_1(P)$ ($e^3t_2^5$) excited states. With a trigonal distortion (lowering to C_{3v} symmetry), the $^3T_1$ states split into $^3A_2$ (ground state; $e^4A_1^2e^2$ in a C_{3v} strong field representation) and ^3E, and the $^3T_2$ state into $^3A_1$ ($e^3a_1^2e^3$) and ^3E (the ^3E states are not conveniently described using a strong field notation).

The specific example here comprises Ni(II) complexes of general formula L_3NiX, where L is a monodentate ligand or the pyrazolyl group of a scorpionate (i.e., TpNiX) and X is a (pseudo)halide ion. These complexes have idealized C_{3v} point group symmetry and their structures are analogous to that shown in Fig. 7 (inset). The ground state is $^3A_2$ [from $^3T_1(F)$]; there is a low-lying ^3E excited state with the same parentage and then the other triplet excited states follow as given above. In this case, the most convenient description is to use the MO scheme: $(1e)^4(a_1)^2(2e)^2$, where MO $1e$ involves the $d_{x^2-y^2}$ and d_{xy} ($d_{\pm 2}$) orbitals, MO a_1 the d_{z^2} (d_0) orbital, and MO $2e$ involves the d_{xz} and d_{yz} ($d_{\pm 1}$) orbitals. However, as they have the same symmetry, $1e$ includes significant contributions from d_{xy} and d_{xy} and vice versa for $2e$. Moreover, there are also contributions to these Ni $3d$ orbitals from the X ligand np orbitals of appropriate symmetry (e.g., np_z contributes to a_1, and $np_{x,\,y}$ to $1e$ and $2e$). This effect of X was ignored in the opening discussion (the effect of contributions from orbitals of the other ligand(s), e.g., pyrazole N $2s,p$ in TpNiX, is not crucial).

The case of L_3NiX was studied computationally in detail by Ye and Neese [121], based on experimental results for Tp*NiX (Tp* = hydridotris(3,5-dimethyl-pyrazol-1-yl)borate anion; the methyl groups were truncated for the calculations) from HFEPR and other techniques [86]. Ye and Neese [94, 121, 130] used wavefunction-based ab initio methods: state-averaged complete active space self-consistent field (CASSCF), second-order N-electron valence perturbation theory (NEVPT2), and spectroscopy oriented configuration interaction (SORCI). The nature of these methods is beyond us, but a key point is that standard DFT methods are not sufficient for a problem of this complexity [124].

Moreover, we will not reproduce their results, but simply state that the work by Ye and Neese [121] represents a paradigm for elucidating the chemical origins and significance of zfs. In particular, we direct the interested reader towards their Table 4, which summarizes the contributions to zfs from a host of electronic transitions, analogous to the discussion in the above section. They list nine such transitions, of which only four (the same for each of X = Cl, Br, I) have SOC contributions to D that are larger than 1 cm^{-1} in magnitude (SSC was also negligible in these systems). These transitions are as follows (with very rough consensus values for the contribution to D also provided): two spin-allowed transitions: $^3A_2 \rightarrow {}^3A_1$ ($1e \rightarrow 2e$; -60 cm^{-1}) and $^3A_2 \rightarrow {}^3E$ ($1a_1 \rightarrow 2e$; $+50$ cm^{-1}), and two spin-forbidden transitions: $^3A_2 \rightarrow {}^1A_1$ ($2e \rightarrow 2e$ spin-flip; $+10$ cm^{-1}) and $^3A_2 \rightarrow {}^1E$ ($1a_1 \rightarrow 2e$ spin-flip; -10 cm^{-1}). It is thus easy to see that, although there can be very large individual contributions to zfs, because they can be opposite in sign (as was true for $D_{^5B_2}$ and $D_{^5E}$ in the d^4 case above), the overall zfs can be small in magnitude, and may even change sign in a related series of complexes, as is the case for TpNiX.

Another point is the experimentally observed wide variation in zfs as a function of X ligand [86]. The $[Ni^{II}–X]^+$ unit has a "resonance" form $[Ni^{I}–X^{\bullet}]^+$, i.e., significant spin delocalization onto the halido ligand. Because ζ for iodine is nearly an order of magnitude larger than it is for chlorine, zfs from the relevant electronic excited states can vary greatly depending on the degree of ligand covalency in each.

Practical aspects of HFEPR spectroscopy

Differences between conventional EPR and HFEPR

The extension of the operating frequency range up to 1 THz and that of the magnetic field up to 25 T or higher have far-reaching consequences for the sensitivity and applicability of the technique, as briefly mentioned in the "General overview" section. This has two reasons: physics and technology. On the physical side, the increase in frequency and field in spin systems where magnetic anisotropy is principally determined by g-anisotropy causes the absorption to spread over the field scale, reducing its amplitude (it should be recalled that the features observed in powder EPR spectra are turning points only, i.e., distinct edges of the absorption, not absorption per se). Since the width of the turning points generally also increases with frequency and field due to phenomena such as g-strain, this causes a further decrease in signal amplitude. In spin systems where magnetic anisotropy is principally caused by zfs, similar phenomena occur, even if the actual pattern of

resonances is not directly frequency or field dependent. In particular, there is a large difference between Kramers and non-Kramers spin systems. In the former case, there is always one Kramers doublet ($M_S = \pm 1/2$) within which it is almost guaranteed to observe an allowed ($\Delta M_S = \pm 1$) transition independently of frequency or field. In the latter case, interdoublet transitions are primarily observed, and these very strongly depend on the combination of frequency and field, which often results in such systems being EPR-silent in conventional EPR. This explains why it is much easier to do EPR (including HFEPR) on Kramers systems such as Mn(II), Fe(III), or Co(II) than on non-Kramers ions such as Mn(III), Fe(II), or Fe(IV).

The second reason for the relative decrease of sensitivity in HFEPR relative to X- or Q-band EPR has to do with the technology. As the operating frequencies have moved from the GHz regime to the sub-THz one, microwave techniques of generating, propagating, and detecting the electromagnetic radiation have increasingly failed. In particular, transmission losses in conventional waveguides have become prohibitive, forcing the use of oversized pipelines or free-space propagation. Even more importantly, resonant cavities become impractically small with decreasing wavelength. The current limit for cavity application is ca. 300 GHz, and resonators operating close to that value can accommodate only minute amounts of sample. Oversized cavities such as those of the Fabry–Perot type have proved impractical. It is thus necessary to give up on resonators and work in pure transmission (or reflection) mode. It should be noted that in such a case one can increase the sample volume, which at least partly compensates for the loss of sensitivity due to the lack of a resonator. In fact, were it not for the physical effects described in the previous paragraph, the overall (or concentration) sensitivity of the transmission setup as routinely used at the NHMFL would not be much lower, if at all, than that of conventional X-band spectrometers.

Sample form and concentration

Given the above considerations, it should not be a surprise that a majority of bioinorganically relevant spin systems studied by HFEPR comprise biomimetic models rather than actual biological systems such as metalloenzymes. This has mostly to do with the concentration: for many synthetic complexes it is possible to work with powders, or with highly concentrated solutions in a solvent of choice. With the biological samples, success strongly depends on the particular spin system selected: while concentrations of a fraction of mM either in water or organic solvent can be sufficient for Kramers ions, which makes it possible to study metalloenzymes containing Mn(II) or Fe(III), this is rarely possible with non-Kramers spin systems. The only solution HFEPR metalloprotein study so far of a non-Kramers metal ion, Fe(II) in Rd-red [90], necessitated a 10 mM concentration of the protein; the same concentration was used for oxidized desulforedoxin [70]. Not many metalloproteins can be concentrated to such a degree.

A considerable variety of HFEPR spectrometers—most of them homemade—exist worldwide. Limiting our description to only a single location, namely the NHMFL in Tallahassee, it is still not feasible to offer their full characteristics. The NHMFL-based instrumentation is described in detail online [133]. Also, a hands-on description of HFEPR and its practical requirements with regard to sample form and preparation was provided by some of us in the International EPR (ESR) Society newsletter [134], and is freely available from the authors upon request. The reader is directed to these resources if planning or contemplating an actual experiment at the NHMFL or another HFEPR laboratory. In general, it should be emphasized that HFEPR experiments can be very different from single-frequency X- or Q-band measurements, as the differences in the frequencies and magnetic field range involved place varying constraints on the sample form and volume, as well as the acquisition time involved.

Simulation and other software

Interpreting raw HFEPR (or any EPR) data requires adequate software. Luckily, there is an abundance of such software in the world these days, much of which is available free of charge (although the commercial program Xsophe from Bruker Biospin is not), starting with SPIN, which is available from A. Ozarowski. Other programs, such as SIM by H. Weihe [135], Easy Spin[2] by Stoll [136, 137], and Spin Count by Hendrich [138], are readily applicable to the analysis and simulation of HFEPR spectra with the purpose of extracting spin Hamiltonian parameters. Once these parameters have been deduced, obtaining chemically useful information is the next step, as discussed above in the "Relation between spin Hamiltonian parameters and bonding information" section.

Conclusions and outlook

One can consider HFEPR in the context of other spectroscopic methods that give information on the zfs of paramagnetic bioinorganic systems: VTVH-MCD, VTVH-Mössbauer, and magnetometry. MCD is a very

[2] EasySpin is a MATLAB® toolbox for simulating and fitting EPR spectra. EasySpin runs on a variety of operating systems and is available free of charge; see: http://www.easyspin.org/.

powerful technique for providing information on electronic transitions, quite apart from spin Hamiltonian parameters, and requires relatively low concentrations. However, optical quality glasses are needed as well as detectable bands in the visible. VTVH-Mössbauer is also very powerful in terms of providing oxidation state and quadrupole and hyperfine coupling information that is not easily obtained from EPR. Also, provided sufficient enrichment in ^{57}Fe is present, it gives dependable results. It is of course limited to ^{57}Fe (among biologically relevant Mössbauer active nuclei). Magnetic susceptibility likewise gives good if not always very accurate results, but is very difficult to investigate for biological solutions and, even for solids, its measurement is fraught with difficulties/inaccuracies because it is a bulk property measurement, not a resonant technique. HFEPR, as we hope that we have demonstrated here, is applicable to a wide range of spin systems and, when sufficient quality spectra are obtained, it can provide the complete set of spin Hamiltonian parameters with an accuracy and precision that is unmatched by other methods. However, we emphasize in the strongest terms that HFEPR is not a substitute for but a complement to techniques such as MCD and Mössbauer, as well as to X-ray crystallography and NMR. Equally important is that the parameters obtained from HFEPR are not an end in themselves, but instead are the experimental "reality" that provides the target for theory to achieve. While it would be presumptuous to claim that HFEPR is solely responsible for inspiring recent developments in computational methods as applied to open-shell systems, it is the case that the data now available on a wide range of $S > 1/2$ transition metal complexes have motivated the development and implementation of ab initio methods, as pioneered for transition metal systems by Neese and co-workers and described in detail by them [123, 124, 130, 139]. Such quantum chemistry calculations provide a complete picture of the electronic structure of a bioinorganic system and relate this to reactivity [56].

We therefore conclude with a plea to workers in bioinorganic chemistry, whether with metalloproteins or model compounds, to consider HFEPR investigations of any systems that they encounter that contain $S > 1/2$ centers, whether of mono- or higher nuclearity.

Acknowledgments The NHMFL is funded by the NSF through Cooperative Agreement DMR 1157490, the State of Florida, and the DOE. We thank Prof. Mahdi M. Abu-Omar and Dr. Scott Hicks, Purdue University, for the [Mn(tpfc)] sample, and Prof. Brian M. Hoffman and Dr. Judith A. Nocek, Northwestern University, for the met-Mb-F sample. The [Tp^{tBu}Ni(NCS)] and [Tp^{tBu,Np}CoN$_3$] samples originated with the late Dr. S. Trofimenko, University of Delaware. We thank Prof. Timothy A. Jackson, University of Kansas, for helpful comments.

References

1. Que L Jr (2000) Physical methods in bioinorganic chemistry: spectroscopy and magnetism. University Science Books, Sausalito
2. Sahu ID, McCarrick RM, Lorigan GA (2013) Biochemistry 52:5967–5984. doi:10.1021/bi400834a
3. Drago RS (1992) Physical methods for chemists. Saunders College, Ft. Worth
4. Abragam A, Bleaney B (1986) Electron paramagnetic resonance of transition ions. Dover, Mineola
5. Poole CP (1996) Electron spin resonance. Dover, Mineola
6. Weil JA, Bolton JR (2007) Electron paramagnetic resonance: elementary theory and practical applications. Wiley, Hoboken
7. Weltner W Jr (1983) Magnetic atoms and molecules. Dover, Mineola
8. Hanson G, Berliner L (eds) (2010) Metals in biology: applications of high-resolution EPR to metalloenzymes. Springer, New York
9. Hanson G, Berliner L (eds) (2009) High resolution EPR: applications to metalloenzymes and metals in medicine. Springer, New York
10. Andersson KK, Schmidt PP, Katterle B, Strand KR, Palmer AE, Lee S-K, Solomon EI, Gräslund A, Barra A-L (2003) J Biol Inorg Chem 8:235–247. doi:10.1007/s00775-002-0429-0
11. Grinberg O, Berliner LJ (eds) (2004) Very high frequency (VHF) ESR/EPR. Springer, New York
12. Morley GW, Brunel L-C, Tol Jv (2008) Rev Sci Instrum 79:064703. doi:10.1063/1.2937630
13. Takahashi S, Brunel LC, Edwards DT, van Tol J, Ramian G, Han S, Sherwin MS (2012) Nature 489:409–413. doi:10.1038/nature11437
14. Stoll S (2010) In: Gilbert BC, Murphy DM, Chechik V (eds) Electron paramagnetic resonance. Royal Society of Chemistry, London, pp 107–154. doi:10.1039/9781849730877-00107
15. Sofia HJ, Chen G, Hetzler BG, Reyes-Spindola JF, Miller NE (2001) Nucleic Acids Res 29:1097–1106. doi:10.1093/nar/29.5.1097
16. Booker SJ (2012) Biochim Biophys Acta Proteins Proteomics 1824:1151–1153. doi:10.1016/j.bbapap.2012.07.006
17. Wiig JA, Hu Y, Lee CC, Ribbe MW (2012) Science 337:1672–1675. doi:10.1126/science.1224603
18. Blankenship RE (2002) Molecular mechanisms of photosynthesis. Blackwell, Oxford
19. Yukl ET, Liu F, Krzystek J, Shin S, Jensen LMR, Davidson VL, Wilmot CM, Liu A (2013) Proc Natl Acad Sci USA 110:4569–4573. doi:10.1073/pnas.1215011110
20. Stoll S, Shafaat HS, Krzystek J, Ozarowski A, Tauber MJ, Kim JE, Britt RD (2011) J Am Chem Soc 133:18098–18101. doi:10.1021/ja208462t
21. Rieger PH (1994) Coord Chem Rev 135–136:203–286. doi:10.1016/0010-8545(94)80069-3
22. McGarvey BR (1998) Coord Chem Rev 170:75–92. doi:10.1016/S0010-8545(97)00073-8
23. Walker FA (1999) Coord Chem Rev 185–186:471–534. doi:10.1016/S0010-8545(99)00029-6
24. Boča R (2004) Coord Chem Rev 248:757–815. doi:10.1016/j.ccr.2004.03.001
25. Neese F (2009) Coord Chem Rev 253:526–563. doi:10.1016/j.ccr.2008.05.014
26. Neese F (2006) J Am Chem Soc 128:10213–10222. doi:10.1021/ja061798a
27. Bendix J, Brorson M, Schäffer CE (1993) Inorg Chem 32:2838–2849. doi:10.1021/ic00065a010

28. McGavin DG, Tennant WC, Weil JA (1990) J Magn Reson 87:92–109. doi:10.1016/0022-2364(90)90088-Q
29. McGavin DG (1987) J Magn Reson 74:19–55. doi:10.1016/0022-2364(87)90077-1
30. Crouse BR, Meyer J, Johnson MK (1995) J Am Chem Soc 117:9612–9613. doi:10.1021/ja00142a049
31. Knapp MJ, Krzystek J, Brunel L-C, Hendrickson DN (1999) Inorg Chem 38:3321–3328. doi:10.1021/ic9901012
32. Zein S, Duboc C, Lubitz W, Neese F (2008) Inorg Chem 47:134–142. doi:10.1021/ic701293n
33. Krzystek J, Ozarowski A, Telser J (2006) Coord Chem Rev 250:2308–2324. doi:10.1016/j.ccr.2006.03.016
34. Krzystek J, Zvyagin SA, Ozarowski A, Trofimenko S, Telser J (2006) J Magn Reson 178:174–183. doi:10.1016/j.jmr.2005.09.007
35. Telser J, Ozarowski A, Krzystek J (2013) Electron paramagnetic resonance, vol 23. The Royal Society of Chemistry, London, pp 209–263. doi:10.1039/9781849734837-00209
36. Venters RA, Nelson MJ, McLean PA, True AE, Levy MA, Hoffman BM, Orme-Johnson WH (1986) J Am Chem Soc 108:3487–3498. doi:10.1021/ja00272a054
37. True AE, Nelson MJ, Venters RA, Orme-Johnson WH, Hoffman BM (1988) J Am Chem Soc 110:1935–1943. doi:10.1021/ja00214a045
38. Wallar BJ, Lipscomb JD (1996) Chem Rev 96:2625–2658. doi:10.1021/cr9500489
39. Solomon EI, Brunold TC, Davis MI, Kemsley JN, Lee S-K, Lehnert N, Neese F, Skulan AJ, Yang Y-S, Zhou J (2000) Chem Rev 100:235–350. doi:10.1021/cr9900275
40. Que L Jr (2007) Acc Chem Res 40:493–500. doi:10.1021/ar700024g
41. Tinkham M (1956) Proc R Soc Lond A 236:535–548. doi:10.1098/rspa 1956.0154
42. Tinkham M (1956) Proc R Soc Lond A 236:549–563. doi:10.1098/rspa.1956.0155
43. Hu C, Sulok CD, Paulat F, Lehnert N, Twigg AI, Hendrich MP, Schulz CE, Scheidt WR (2010) J Am Chem Soc 132:3737–3750. doi:10.1021/ja907584x
44. Münck E, Surerus KK, Hendrich MP (1993) Meth Enzym Part D 227:463–479. doi:10.1016/0076-6879(93)27019-D
45. Hendrich MP, Debrunner PG (1989) Biophys J 56:489–506. doi:10.1016/S0006-3495(89)82696-7
46. Hendrich MP, Gunderson W, Behan RK, Green MT, Mehn MP, Betley TA, Lu CC, Peters JC (2006) Proc Natl Acad Sci USA 103:17107–17112. doi:10.1073/pnas.0604402103
47. Gupta R, Lacy DC, Bominaar EL, Borovik AS, Hendrich MP (2012) J Am Chem Soc 134:9775–9784. doi:10.1021/ja303224p
48. Campbell KA, Yikilmaz E, Grant CV, Gregor W, Miller A-F, Britt RD (1999) J Am Chem Soc 121:4714–4715. doi:10.1021/ja9902219
49. Fann Y-C, J-l Ong, Nocek JM, Hoffman BM (1995) J Am Chem Soc 117:6109–6116. doi:10.1021/ja00127a025
50. Aasa R (1970) J. Chem. Phys. 52:3919–3930. doi:10.1063/1.1673591
51. Weisser JT, Nilges MJ, Sever MJ, Wilker JJ (2006) Inorg Chem 45:7736–7747. doi:10.1021/ic060685p
52. Gatteschi D, Barra AL, Caneschi A, Cornia A, Sessoli R, Sorace L (2006) Coord Chem Rev 250:1514–1529. doi:10.1016/j.ccr.2006.02.006
53. Telser J, Wu C–C, Chen K-Y, Hsu H-F, Smirnov D, Ozarowski A, Krzystek J (2009) J Inorg Biochem 102:487–495. doi:10.1016/j.jinorgbio.2009.01.016
54. Melchior M, Rettig SJ, Liboiron BD, Thompson KH, Yuen VG, McNeill JH, Orvig C (2001) Inorg Chem 40:4686–4690. doi:10.1021/ic000984t
55. Krzystek J, England J, Ray K, Ozarowski A, Smirnov D, Que L Jr, Telser J (2008) Inorg Chem 47:3483–3485. doi:10.1021/ic800411c
56. Usharani D, Janardanan D, Li C, Shaik S (2013) Acc Chem Res 46:471–482. doi:10.1021/ar300204y
57. Craft JL, Horng Y-C, Ragsdale SW, Brunold TC (2004) J Biol Inorg Chem 9:77–89. doi:10.1007/s00775-003-0499-7
58. Wojciechowska A, Daszkiewicz M, Staszak Z, Trusz-Zdybek A, Bieńko A, Ozarowski A (2011) Inorg Chem 50:11532–11542. doi:10.1021/ic201471f
59. Wojciechowska A, Gągor A, Duczmal M, Staszak Z, Ozarowski A (2013) Inorg Chem 52:4360–4371. doi:10.1021/ic3024919
60. Li Y, Zamble DB (2009) Chem Rev 109:4617–4643. doi:10.1021/cr900010n
61. Trofimenko S (1999) Scorpionates: the coordination chemistry of polypyrazolylborate ligands. Imperial College, London
62. Trofimenko S (2004) Polyhedron 23:197–203. doi:10.1016/j.poly.2003.11.013
63. McNaughton RL, Roemelt M, Chin JM, Schrock RR, Neese F, Hoffman BM (2010) J Am Chem Soc 132:8645–8656. doi:10.1021/ja1004619
64. Wu AJ, Penner-Hahn JE, Pecoraro VL (2004) Chem Rev 104:903–938. doi:10.1021/cr020627v
65. Cox N, Pantazis DA, Neese F, Lubitz W (2013) Acc Chem Res 46:1588–1596. doi:10.1021/ar3003249
66. McConnell IL, Grigoryants VM, Scholes CP, Myers WK, Chen P-Y, Whittaker JW, Brudvig GW (2012) J Am Chem Soc 134:1504–1512. doi:10.1021/ja203465y
67. Duboc C, Collomb M-N (2009) Chem Commun 2715–2717. doi:10.1039/B901185D
68. Larrabee JA, Alessi CM, Asiedu ET, Cook JO, Hoerning KR, Klingler LJ, Okin GS, Santee SG, Volkert TL (1997) J Am Chem Soc 119:4182–4196. doi:10.1021/ja963555w
69. Maret W, Vallee BL (1993) Methods Enzymol 226:52–71. doi:10.1016/0076-6879(93)26005-T
70. Mathies G, Almeida RM, Gast P, Moura JJG, Groenen EJJ (2012) J Phys Chem B 116:7122–7128. doi:10.1021/jp3025655
71. Krzystek J, Swenson DC, Zvyagin SA, Smirnov D, Ozarowski A, Telser J (2010) J Am Chem Soc 132:5241–5253. doi:10.1021/ja910766w
72. Atanasov M, Neese F, Telser J, Krzystek J, Ozarowski A, Larrabee JA, Swenson DC (2014) (in progress)
73. Titiš J, Boča R (2011) Inorg Chem 50:11838–11845. doi:10.1021/ic202108j
74. Tomkowicz Z, Ostrovsky S, Foro S, Calvo-Perez V, Haase W (2012) Inorg Chem 51:6046–6055. doi:10.1021/ic202529p
75. Hadler KS, Mitić N, Yip SH-C, Gahan LR, Ollis DL, Schenk G, Larrabee JA (2010) Inorg Chem 49:2727–2734. doi:10.1021/ic901950c
76. Larrabee JA, Johnson WR, Volwiler AS (2009) Inorg Chem 48:8822–8829. doi:10.1021/ic901000d
77. Watterson SJ, Mitra S, Swierczek SI, Bennett B, Holz RC (2008) Biochemistry 47:11885–11893. doi:10.1021/bi801499g
78. Larrabee JA, Leung CH, Moore RL, Thamrong-nawasawat T, Wessler BSH (2004) J Am Chem Soc 126:12316–12324. doi:10.1021/ja0485006
79. Šebová M, Boča R, Dlháň Ľ, Nemec I, Papánková B, Pavlik J, Fuess H (2012) Inorg Chim Acta 383:143–151. doi:10.1016/j.ica.2011.10.073
80. Barra A-L, Døssing A, Morsing T, Vibenholt J (2011) Inorg Chim Acta 373:266–269. doi:10.1016/j.ica.2011.02.024
81. Horitani M, Yashiro H, Hagiwara M, Hori H (2008) J Inorg Biochem 102:781–788. doi:10.1016/j.jinorgbio.2007.11.015
82. Hori H, Yashiro H, Ninomiya K, Horitani M, Kida T, Hagiwara M (2011) J Inorg Biochem 105:1596–1602. doi:10.1016/j.jinorgbio.2011.09.007

83. Krzystek J, Telser J (2003) J Magn Reson 162:454–465. doi:10.1016/S1090-7807(03)00042-9
84. Krzystek J, Pardi LA, Brunel L-C, Goldberg DP, Hoffman BM, Licoccia S, Telser J (2002) Spectrochim Acta A 58:1113–1127. doi:10.1016/S1386-1425(01)00701-6
85. Edwards NY, Eikey RA, Loring MI, Abu-Omar MM (2005) Inorg Chem 44:3700–3708. doi:10.1021/ic0484506
86. Desrochers PJ, Telser J, Zvyagin SA, Ozarowski A, Krzystek J, Vicic DA (2006) Inorg Chem 45:8930–8941. doi:10.1021/ic060843c
87. Andino JG, Kilgore UJ, Pink M, Ozarowski A, Krzystek J, Telser J, Baik M-H, Mindiola DJ (2010) Chem Sci 1:351–356. doi:10.1039/c0sc00201a
88. Beinert H (2000) J Biol Inorg Chem 5:2–15. doi:10.1007/s007750050002
89. Knapp MJ, Krzystek J, Brunel L-C, Hendrickson DN (2000) Inorg Chem 39:281–288. doi:10.1021/ic9910054
90. Barra AL, Hassan AK, Janoschka A, Schmidt CL, Schünemann V (2006) Appl Magn Reson 30:385–397. doi:10.1007/BF03166208
91. Costas M, Mehn MP, Jensen MP, Que L Jr (2004) Chem Rev 104:939–986. doi:10.1021/cr020628n
92. England J, Martinho M, Farquhar ER, Frisch JR, Bominaar EL, Münck E, Que L Jr (2009) Angew Chem Int Ed 48:3622–3626. doi:10.1002/anie.200900863
93. Vallejo J, Pascual-Álvarez A, Cano J, Castro I, Julve M, Lloret F, Krzystek J, Munno GD, Armentano D, Wernsdorfer W, Ruiz-García R, Pardo E (2013) Angew Chem Int Ed 52:14075–14079. doi:10.1002/anie.201308047
94. Duboc C, Ganyushin D, Sivalingam K, Collomb M-N, Neese F (2010) J Phys Chem A 114:10750–10758. doi:10.1021/jp107823s
95. Cotruvo JA Jr, Stubbe J (2011) Biochemistry 50:1672–1681. doi:10.1021/bi101881d
96. Cotruvo JA Jr, Stich TA, Britt RD, Stubbe J (2013) J Am Chem Soc 135:4027–4039. doi:10.1021/ja312457t
97. Tabares LC, Cortez N, Un S (2007) Biochemistry 46:9320–9327. doi:10.1021/bi700438j
98. Tabares LC, Cortez N, Agalidis I, Un S (2005) J Am Chem Soc 127:6039–6047. doi:10.1021/ja047007r
99. Un S, Tabares LC, Cortez N, Hiraoka BY, Yamakura F (2004) J Am Chem Soc 126:2720–2726. doi:10.1021/ja036503x
100. Un S, Dorlet P, Voyard G, Tabares LC, Cortez N (2001) J Am Chem Soc 123:10123–10124. doi:10.1021/ja016258m
101. Tabares LC, Gätjens J, Hureau C, Burrell MR, Bowater L, Pecoraro VL, Bornemann S, Un S (2009) J Phys Chem B 113:9016–9025. doi:10.1021/jp9021807
102. Angerhofer A, Moomaw EW, García-Rubio I, Ozarowski A, Krzystek J, Weber RT, Richards NGJ (2007) J Phys Chem B 111:5043–5046. doi:10.1021/jp0715326
103. Moomaw EW, Angerhofer A, Moussatche P, Ozarowski A, García-Rubio I, Richards NGJ (2009) Biochemistry 48:6116–6125. doi:10.1021/bi801856k
104. Mathies G, Blok H, Disselhorst JAJM, Gast P, Meer Hvd, Miedema DM, Almeida RM, Moura JJG, Hagen WR, Groenen EJJ (2011) J Magn Reson 210:126–132. doi:10.1016/j.jmr.2011.03.009
105. Biaso F, Duboc C, Barbara B, Serratrice G, Thomas F, Charapoff D, Béguin C (2005) Eur J Inorg Chem 467–478. doi:10.1002/ejic.200400414
106. van Kan PJM, van der Horst E, Reijerse EJ, van Bentum PJM, Hagen WR (1998) J Chem Soc Faraday Trans 94:2975–2978. doi:10.1039/A803058H
107. Nehrkorn J, Martins BM, Holldack K, Stoll S, Dobbek H, Bittl R, Schnegg A (2013) Mol Phys 111:2696–2707. doi:10.1080/00268976.2013.809806
108. Brackett GC, Richards PL, Caughey WS (1971) J Chem Phys 54:4383–4401. doi:10.1063/1.1674688
109. Solomon EI, Sarangi R, Woertink JS, Augustine AJ, Yoon J, Ghosh S (2007) Acc Chem Res 40:581–591. doi:10.1021/ar600060t
110. Balasubramanian R, Rosenzweig AC (2007) Acc Chem Res 40:573–580. doi:10.1021/ar700004s
111. Reger DL, Pascui AE, Smith MD, Jezierska J, Ozarowski A (2012) Inorg Chem 51:11820–11836. doi:10.1021/ic301757g
112. Reger DL, Pascui AE, Smith MD, Jezierska J, Ozarowski A (2012) Inorg Chem 51:7966–7968. doi:10.1021/ic301321r
113. Reger DL, Debreczeni A, Smith MD, Jezierska J, Ozarowski A (2012) Inorg Chem 51:1068–1083. doi:10.1021/ic202198k
114. Ozarowski A, Szymańska IB, Muzioł T, Jezierska J (2009) J Am Chem Soc 131:10279–10292. doi:10.1021/ja902695y
115. Sharma RP, Saini A, Monga D, Venugopalan P, Jezierska J, Ozarowski A, Ferretti V (2014) New J Chem 38:437–447. doi:10.1039/C3NJ00736G
116. Cutsail GE III, Doan PE, Hoffman BM, Meyer J, Telser J (2012) J Biol Inorg Chem 17:1137–1150. doi:10.1007/s00775-012-0927-7
117. Smoukov SK, Quaroni L, Wang X, Doan PE, Hoffman BM, Que L Jr (2002) J Am Chem Soc 124:2595–2603. doi:10.1021/ja003169l
118. Smoukov SK, Kopp DA, Valentine AM, Davydov R, Lippard SJ, Hoffman BM (2002) J Am Chem Soc 124:2657–2663. doi:10.1021/ja010123z
119. Smoukov SK, Davydov RM, Doan PE, Sturgeon B, Kung I, Hoffman BM, Kurtz DMJ (2003) Biochemistry 42:6201–6208. doi:10.1021/bi0300027
120. Christianson DW (2005) Acc Chem Res 38:191–201. doi:10.1021/ar040183k
121. Ye S, Neese F (2012) J Chem Theory Comput 8:2344–2351. doi:10.1021/ct300237f
122. Mossin S, Weihe H, Barra A-L (2002) J Am Chem Soc 124:8764–8765. doi:10.1021/ja012574p
123. Ganyushin D, Neese F (2006) J Chem Phys 125:024103. doi:10.1063/1.2213976
124. Neese F (2006) J Biol Inorg Chem 11:702–711. doi:10.1007/s00775-006-0138-1
125. Atanasov M, Ganyushin D, Sivalingam K, Neese F (2012) In: Mingos DMP, Day P, Dahl JP (eds) Molecular electronic structures of transition metal complexes II. Springer, Berlin, pp 149–220
126. Atanasov M, Ganyushin D, Pantazis DA, Sivalingam K, Neese F (2011) Inorg Chem 50:7460–7477. doi:10.1021/ic200196k
127. Ganyushin D, Neese F (2013) J Chem Phys 138:104113. doi:10.1063/1.4793736
128. Sandhoefer B, Kossmann S, Neese F (2013) J Chem Phys 138:104102. doi:10.1063/1.4792362
129. Neese F (2012) Wiley Interdiscip Rev Comput Mol Sci 2:73–78. doi:10.1002/wcms.81
130. Neese F, Petrenko T, Ganyushin D, Olbrich G (2007) Coord Chem Rev 251:288–327. doi:10.1016/j.ccr.2006.05.019
131. Krzystek J, Telser J, Pardi LA, Goldberg DP, Hoffman BM, Brunel L-C (1999) Inorg Chem 38:6121–6129. doi:10.1021/ic9901970
132. McGarvey BR (1966) In: Carlin RL (ed) Transition metal chemistry. Marcel Dekker, New York, pp 89–201
133. NHMFL (2014) Electron magnetic resonance (EMR) overview. NHMFL, Tallahassee. http://magnet.fsu.edu/usershub/scientificdivisions/emr/index.html. Accessed 20 Dec 2013
134. Krzystek J, Ozarowski A, van Tol J, Liu J, Hill S (2012) EPR Newsl 22:12–14 (this is available from the authors upon request)
135. Weihe H (2003) SIM. University of Copenhagen, Copenhagen
136. Stoll S (2013) EasySpin. University of Washington, Seattle
137. Stoll S, Schweiger A (2006) J Magn Reson 178:42–55. doi:10.1016/j.jmr.2005.08.013
138. Hendrich M (2013) Spin Count. Carnegie-Mellon University, Pittsburgh
139. Kirchner B, Wennmohs F, Ye S, Neese F (2007) Curr Opin Chem Biol 11:134–141. doi:10.1016/j.cbpa.2007.02.026